In situ synthesis of Ti_xAl_y-Al_2O_3 composites

By

K Venkata Ramaiah

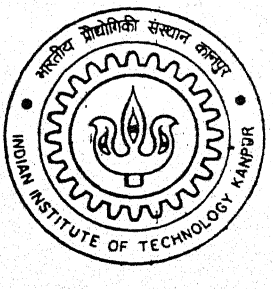

DEPARTMENT OF MATERIALS AND METALLURGICAL ENGINEERING

Indian Institute of Technology Kanpur

JANUARY, 2002

In situ synthesis of Ti_xAl_y-Al_2O_3 composites

A Thesis submitted

in partial fulfillment of the requirements

for the degree of

Master of Technology

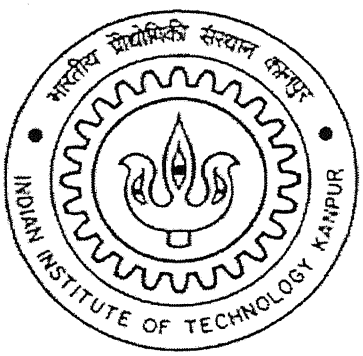

by

K Venkata Ramaiah

to the

Department of Materials and Metallurgical Engineering

Indian Institute of Technology Kanpur

- 5 MAR 2002/MME
पुरुषोत्तम कार्तिकेय वेंकटरमन पुस्तकालय
भारतीय प्रौद्योगिकी संस्थान कानपुर
अवाप्ति क्र० A 137951

ACKNOWLEDGEMENTS

I wish to register my grateful thanks to my thesis supervisors, Prof. V.S.R. Murthy and Dr. Asim Tewari. Their keen interest on my work and me has made this thesis possible. I am grateful to them for their guidance, inspiration, constant encouragement and help, which often extended beyond the academic. I would like to specially thank Dr. Asim Tewari, for physically involved in thesis writing and formating.

I wish to thank Mr. R. K. Prasad and several lab colleagues for their cooperation and assistance in solving experimental related difficulties.

Finally, I would like to thank all of my friends who helped me, directly or indirectly in successful completion of this project.

K VENKATA RAMAIAH

I.I.T. KANPUR

LIST OF SYMBOLS

T_i	Ignition temperature
t_I	Time of ignition, respectively;
η	Degree of advancement of reaction
ΔH_r	Enthalpy of the reaction
k	Reaction rate constant at the ignition temperature
λ_{eff}	Effective thermal conductivity of the bed of particulate reactants
r	Radial position
P	Load at the failure
b	Breadth of the beam specimen
w	Width of the beam speimen
d_1	Inner span length
d_2	Outer span length
a	Notch depth of fracture toughness specimen
d_{cr}	Critical grain size
K_{Ic}	Critical fracture toughness in mode I
σ_y	Flexural strength
δ	Relative elongation to fracture
m	Strain rate sensitivity coefficient
MM	Mechanical milling
HP	Hot pressing
HT	Heat treatment
EPMA	Electron Probe Micro Analyzer
XRD	X-ray Diffraction
SEM	Scanning Electron Microscope
DSC	Differential Scanning Calorimeter
3A	Alumina Aluminide Alloys
	Area per area (= volume fraction)
V_V	Volume per volume (volume fraction)
L_A	Length per unit area
S_V	Surface area per volume

CONTENTS

LIST OF TABLES

LIST OF FIGURES

ABSTRACT

A recent variation of classic thermit-based reaction is a novel, pressure-less reaction sintering process for the fabrication of Alumina Aluminide Alloys (3A). The 3A process involves the reaction sintering of intensely milled metal / aluminium or metal oxide / aluminium powder compacts, heat treated in a non-oxidizing atmosphere, to form dense, interpenetrating alumina / aluminide composites. Mechanically milled different composition powders were hot pressed and heat-treated in vacuum for different durations. In this investigation, two aspects, namely, obtaining higher forms of aluminide and ductilisation of Ti_xAl_y $-Al_2O_3$ were investigated taking Ti-Al as a model system. Different aluminides (Ti_xAl_y) were successfully synthesized using 3A process. Flexural strength achieved was varied from 80-345 MPa and Fracture toughness was 4.0 MPa$\sqrt{m}$. Porosity was present in the samples varying from 15-20%. Characterization techniques involved in this study were XRD, EPMA, optical microscopy, microhardness, four point bent test and Image analysis for quantitative microscopy.

CHAPTER 1: INTRODUCTION

A composite may be defined as a material consisting of two or more suitably arranged phases with a separating interface between them. The reinforcement can be in the form of fibers, whiskers, platelets or particulates. Depending on the matrix phase, composites are classified as polymer, metal, intermetallic and ceramic matrix composites [1-2]. While polymer and metal matrix composites are used for low or medium temperature applications, intermetallic and ceramic composites are used mainly for high temperature applications. As internmetallics exhibit mixed characteristics of metals and ceramics (e.g. high melting point, lower density, higher strength, good corrosion and oxidation resistance) they are being considered for many structural applications. The most common processing routes for obtaining intermetallic and ceramic composites are: solid state (liquid state) sintering, hot pressing, hot isostatic pressing (HIP) and chemical vapour infiltration (CVI). These conventional processing methods suffer from certain drawbacks such as slow processing, high cost, residual porosity, detrimental interfacial reactions, poor wettability, high processing temperature and pressure. To overcome some of the inherent problems associated with conventional high-temperature composite processing, a number of *in situ* methods have been developed in the recent past [3-4].

In *in situ* composites, the reinforcements are synthesized by chemical reactions between elements or between element(s) and compound(s). Such methodologies have certain advantages compared to conventional composite processing. Firstly, the *in situ* formed reinforcements are thermodynamically stable in the matrix, leading to less degradation in elevated temperature service conditions. Secondly, the interfaces between matrix and reinforcement are clean resulting in a strong interfacial bonding and finally, the *in situ* formed reinforcement particles are finer in size and their distribution in the matrix is more uniform (with no segregation of reinforcements), yielding better mechanical properties. The most impressive feature about recently developed composites is, the matrix and the reinforcement phases form interpenetrating and interconnected network structure, which is generally not seen in the conventional 'ceramets'.

Keeping the aforementioned advantages in mind, several *in situ* composites with interpenetrating structures of metal and ceramic were developed. These metal-ceramic composites processed via *in situ* reactions are classified based on the reactant phases, namely liquid-gas, liquid-liquid, liquid-solid, solid-gas and solid-solid reactions [3-4]. Classification of the composite processing methods is shown in Table 1.1. However, these established processing routes e.g. directed metal oxidation (DIMOX), co-continuous ceramic composites processing (C^4), reactive metal penetration (RMP) are mainly restricted to the manufacturing of aluminum containing composites [3-8]. For the fabrication of refractory metal or intermetallics composites, methods like gas pressure infiltration, hot extrusion, hot pressing or hot isostatic pressing (HIP) are generally employed but they are expensive. Combustion synthesis or SHS (Self-propagating high temperature synthesis) is an innovative technique to produce intermetallic/ceramic composites [9-11]. The key principle of the process is the conversion of chemical energy to thermal energy. The main advantages of the combustion synthesis process are: efficient utilization of the reaction energy, rapid synthesis and purification due to volatilization of impurities. Combustion synthesis encompasses a large number of themit-based reactions. Themit-based reactions have additional advantages over many of the combustion synthesis reactions. Conventional SHS reactions are mainly based on fine elemental powders whereas thermit-based reactions start with naturally occurring oxides, which are less expensive and more readily available than elemental powders. Additionally, the simultaneous production of multiphases in themit-based reactions makes it possible to produce composite materials with even distribution of phases. A recent variation of this classic themit-based reaction is a novel, pressure-less reaction sintering process for the fabrication of Alumina Aluminide Alloys (3A) [12-13]. The 3A process involves the reaction sintering of intensely milled metal/aluminium or metal oxide/aluminium powder compacts, heat treated in a non-oxidizing atmosphere, to form dense, interpenetrating alumina / aluminide composites. This exiting, new technique has been extended to the development of Ti, Fe, Nb, Mo, Zr and Ni base composites mainly alumina as reinforcing phase. The general reaction between the reactants is,

$$Me_aO_b + Al \rightarrow Me_x Al_y + Al_2O_3 \qquad (1.1)$$

Where Me_aO_b refers to any metal oxide which has a favorable Gibb`s free energy for the above reaction. The main advantages of this process are the fabrication steps are scientifically simple and the ceramic / intermetallic ratio together with the microstructural scale can be tailored by altering the initial size.

In composites produced by 3A process, always MAl_3 (M is Ni, Ti, Fe, Zr, Nb etc.) phase appears as a matrix phase. The aluminides of MAl_3 are all of low melting compounds compared to MAl or M_3Al intermetallics. There is a need to produce more refractory phases to make the composites commercially more viable and competetive. The other inherent limitation of these aluminides is ductility. MAl_3 materials are extremely brittle. However, from the earlier research work that was carried out at the IIT Kanpur and elsewhere it is known that some stoichiometric forms like MAl or M_3Al can be made more ductile by adopting different methodologies [14-17]. For example, the ductility of Ni_3Al was increased from almost 0% to more than 50% by doping with boron. Similarly, TiAl was ductilised to some extent (up to 5-6%) by grain refinement [18-28]. In this investigation, these two aspects, namely, obtaining higher forms of aluminide and ductilisation were investigated taking Ti-Al as a model system.

CHAPTER 2: LITERATURE REVIEW

2.1 Introduction

Self-propagating high-temperature synthesis (SHS) or Combustion synthesis is an innovative technique where refractory metal, intermetallic and ceramic composites are produced by *in situ* chemical reactions [11-13,29-32]. The key principle of this process is conversion of chemical energy to thermal energy. A large amount of heat is generated instantly (in few seconds) and different reactant phases are formed in a short span of time. In this chapter, initially the broad principles of combustion synthesis are outlined. A deviation from combustion synthesis is 3A (Aluminium Aluminide Alloys) process. In 3A process, the reactions are exothermic like in SHS process but are of low intensity. 3A process makes use of cheap oxide powders instead of expensive elemental powders that are generally used in SHS reaction. Additionally, the reaction times in 3A process are much longer compared to conventional combustion synthesis process. The longer times are used to ensure complete reaction of powders. Unlike combustion synthesis, in 3A process, the phases generated attain complete equilibrium due to long reaction times. Moreover, the volume fraction and the distribution of phases could be tailored to specific property requirements by controlling the processing variables. The unique feature of composites processed via 3A process is, the microstructures contain bicontinuous networks of intermetallic and ceramic phases. Such microstructures offer better properties compared to conventional composites.

For example, let us consider Ti-Al system, which is the topic of investigation in this thesis. Alumina reinforced titanium aluminide composites can be generated using 3A process using the following *in situ* chemical reaction:

$$3TiO_2 + 7Al \rightarrow 2Al_2O_3 + 3TiAl \qquad (2.1)$$

In the above reaction, there are two sequential steps. The first step is metallothermic reduction of the oxide to the metal, e.g. $TiO_2 \rightarrow Ti$. The second step is the formation of

the required intermetallic compound or reinforcing ceramic phase i.e. Ti → Ti_xAl_y and Al→ Al_2O_3. So, it is also important to understand the reaction between elemental powders (Ti and Al and other related systems) and the influence of external parameters like reaction time and alloying elements on the evolution of final microstructures. Keeping this in view, the literature is presented in two different sections. In the first half of the literature review, the basic processing, microstructure and mechanical properties of various aluminides obtained by 3A process are summarized. In the later part, the reactions in mechanically milled/alloyed powders are reviewed. Finally, most of the aluminides are brittle in nature. It is important to obtain more ductile phases from the viewpoint of mechanical properties. Keeping this in perspective, recent research methodologies adopted for controlling the brittleness are also reviewed [20-24].

2.2 Basic Principles of Combustion Synthesis

The main trend in materials science and engineering at present is the extension of materials spectrum by using energy- and time-efficient technologies, which are also environmentally friendly. One such attempt is combustion synthesis. The distinct feature of combustion synthesis is utilization of exothermic reactions between reactants until complete conversion of reactants to products occurs in a short time. Recently, several reviews have appeared in the literature covering all major basic observations and fundamental concepts of combustion synthesis [33-35].

The basic principle of combustion synthesis is shown schematically in ***Fig 2.1a.*** The reactant powders are mixed and ignited using a DC source or a high-energy beam. Once initiated, highly exothermic reaction can be self-sustaining and will propagate through the reactant mixture in the form of a combustion wave. As the combustion wave front advances, the reactants are converted to the products. When the ignition takes place, the sample's temperature rises abruptly to a maximum value, which is the adiabatic temperature as shown in ***Fig 2.1b***. Some materials and their adiabatic temperatures during combustion synthesis are shown in ***Table 2.1***. It has been found that ignition can be realized in systems of reactants where the reaction enthalpies are of the order of 100

kJ mole^{-1} or higher. For a spherically symmetric bed of particulate reactants and a single reaction the ignition should occur [32] when:

$$(-\Delta H_r)k(T_i,\eta) > \frac{1}{r^2}\frac{\partial}{\partial r}\left[r^2\lambda_{eff}\frac{\partial T}{\partial r}\right]_{t_i} \qquad (2.2)$$

where T_i and t_i are temperature and time of ignition, respectively; η is the degree of advancement of reaction; ΔH_r is the enthalpy of the reaction in j mol^{-1}; $k(T_i,\eta)$ is the reaction rate constant (mol m^{-3} s^{-1}) at the ignition temperature; λ_{eff} is the effective thermal conductivity of the bed of particulate reactants and r is the radial position. From the Eq. 2.2, it can be seen that the sustainable propagation is possible when the two temperature gradients in the bed remain low. Two major factors are expected to affect temperature gradient in a bed of reacting particles. One is the thermal conductivity of the bed because high conductivity favours high thermal gradients and vice versa. Another factor is the size of reactant particles. In a porous particulate bed, the heat flux from particles increases inversely to the particle size; the smaller the particle size lower will the thermal conductivity of the porous bed. This in turn will affect the temperature gradient. The influence of these factors further varies if liquid is formed during the reaction. For example, in Si + C system, the formation of SiC depends on the incipient liquid formed at the reaction front.

As discussed earlier, once the combustion wave is initiated, the rate of propagation depends on two competing processes. They are heat generation and dissipation. Any changes that are brought in these two heat transfer processes can alter the velocity of the front from a steady state to non-steady state. Depending on the propagation of wave front with time, the combustion process can be divided further into oscillatory or a spin motion (***Fig 2.1c***). In the oscillatory mode, the wave moves in successions of rapid and slow displacements, and in the spin mode, the reaction proceeds in a spiral motion from one end to the other. Generally, oscillation motion can be recognized by formation of layered structures in the final product (***Fig 2.1c***).

Sometimes, the instability of combustion wave can lead the reaction from a steady state to unsteady state, ultimately extinguishing the combustion process. Since instability

can come from insufficient heat generation, weak exothermic reactions are susceptible to extinction (e.g formation of SiC, B_4C and some intermetallics). To sustain such reactions two approaches are adopted. Since the adiabatic temperature is function of the initial temperature of the reactants, preheating of the mixture can help to some extent to push the temperature. This approach is called 'thermal explosion', where the reactant mixture is heated in a furnace at a constant rate, until the combustion reaction takes places. The 3A process reactions come under this category. The second technique, namely 'chemical oven' method, used to ignite weak thermit reactions. In this case, the weak exothermic mixtures are combined with intense exothermic mixtures. For example, low exothermic B and C mixtures can be combined with Ti and B mixtures. Some more examples related to pure intermetallics are given below.

Investigations that were carried out on the preparation of intermetallic compounds were focused on the aluminides of nickel [36-42], copper [43], iron [44,45], titanium [46-57] and zirconium [58]. In addition to aluminides, important material like molybdenum silicide was also produced using combustion synthesis [59,60]. As mentioned earlier, the heat formation in intermetallic compounds is relatively low hence they are processed by the 'thermal explosion' method. Typically, powder mixtures of the metals are heated at a constant rate until spontaneous combustion takes place. Recent investigations on the Al-Ni system have shown that the combustion reaction is influenced by precombustion phase formation driven by solid-state diffusion [36]. It has been demonstrated that the extent of formation of these precombustion phases can influence the mechanism of combustion and consequently the characteristics of the product. This is demonstrated by the difference in the microstructure of the products of combustion of identical powder mixture (25 At.%Al and 75 At.% Ni) heated at different rates. When the reactants are heated at 1°C/min, the product exhibited a porosity of 28%. On the other hand, an identical mixture results in a product with a porosity of 16% when the powder mixture was heated at 5°C/min. These porosity differences are attributed to differences in the extent of liquid phase formation during the combustion reaction. It is also interesting to note that the addition of a small amount of boron (~0.5 at.%) further enhances liquid phase formation and, thus, results in a product with still lower porosity. However, the role

of boron on densification was not clearly defined. Itin et al. [43] investigated the formation of titanium nickelide by the SHS process. When compared to conventionally processed alloys SHS process alloys exhibit good 'shape memory effect'. Similar such effects were also noticed in other shape memory alloys.

In combustion it has been observed that particle size influences not only the rate of the reaction but also the nature of the products formed. During combustion synthesis of Ti_5Si_3, an increase in the size of Ti particles made the combustion wave more unstable [11]. In another study on the combustion synthesis of SiC, it was observed that the size of the Si powder had an effect on the grain size of the resulting SiC [61]. Leaving few examples, it should be mentioned that the effect of particle size of the reactants was not systematically investigated (especially in Ti aluminides).

The most important advantage of SHS process is energy savings. In some cases, the products prepared by SHS are superior to those of prepared by conventional methods. The process can be suitably adopted to synthesize solid solutions, intermetallics, composites and even some metastable phases.

2.3 Alumina Aluminide Alloys using *in situ* exothermic reactions (3A process)

Recently a novel powder metallurgy technique for the low cost manufacturing of Alumina Aluminide Alloys (3A) has been developed. The process involves the reaction sintering of attrition milled powder [14,62] mixtures consisting of cheap raw materials like aluminum, metal oxides (e.g. TiO_2, Fe_2O_3, Nb_2O_5, ZrO_2, etc) and/ or elemental metals (Fe, Ni, Cr, Mo, etc) to produce aluminide/alumina composites with interpenetrating network structures [63-73]. To differentiate these structures from that of conventionally produced composites with isolated particles, a new term 'Metcers' is proposed in the literature. The main advantage of 3A process is that it can be suitably modified to suit industrial production methods. Initially, a preform of milled powders can be prepared and later liquid aluminium can be reactive infiltrated using either gas

pressure or squeeze casting. However, in squeeze casting method, to accomplish complete reaction between different constituents, a post heat treatment cycle is mandatory.

In general, the processing involves attrition milling (usually 7-10 hours) in acetone media using zirconia balls, subsequently dried and passed through a 200 μm sieve. Green samples were formed by uniaxial pressing at 50 MPa followed by static pressing at 900 MPa. Heat treatments up to 1550°C were performed in Ar or in vacuum (10^{-3} bar). Using a powder containing metal oxide and aluminum, the reaction sequence includes the aluminothermic reduction as well as the formation of the corresponding aluminides. Additionally, Al_2O_3 is formed in situ as a product from the reaction between the metal oxide and aluminum. The general reaction scheme is as follows:

$$Me_aO_b + Al \rightarrow \quad Me_x\,Al_y + Al_2O_3 \tag{2.3}$$

where Me_aO_b refers to any metal oxide, which has a favorable Gibbs free energy for the above reaction. The general fabrication routes for 3A materials are shown in the ***Fig 2.2.*** In the first process (route.a), Al is attrition milled with an oxide powder (MeO). Upon reaction sintering, very small volume fraction of aluminium oxidises to alumina, and the rest of the aluminium is utilized in reduction of the oxide powder. The reduced powder further reacts to form an *in situ* aluminide (Me_xAl_y). In the second reaction process (route.b), Al_2O_3, Al and metal (metal is suitably chosen to form a desired aluminide) are mechanically milled and sintered at an appropriate temperature. Most of the aluminium reacts with metal to form respective aluminide, and a small amount of aluminium converts to alumina during processing and increases the total alumina content marginally. In some cases, residual aluminium can also be noticed. Further, by adjusting the starting powder composition, it is possible to vary the final composition of 3A alloys over a wide range.

Different aluminide systems and their enthalpies during the *in situ* reactions are given in ***Table 2.2*** [14]. A controlled balance of the rates of heat generation and heat

dissipation seems to be the important conditions for successful 3A processing. The heat generation rate is dependent on the magnitude of the enthalpy of the reaction and the rate of convertion of reactants to the product; the later is related to the heating rate. There fore slow heating rates are beneficial for these systems, which are associated with a large exothermic heat of formation. Phase change thermodynamic properties of oxides of interest are shown in ***Table 2.3***. Transition temperature and heat of transition of different oxides of titanium are available in the following table.

The aluminide/ Al_2O_3 volume ratio can be tailored in a broad range up to ~60 vol % aluminides. It was hypothesized that the fine Al_2O_3 grain size is the main driving force for complete densification of composite on pressureless sintering. The results further indicate that all thermal and compositional treatments known within the intermetallic community can be applied to control the mechanical behavior of the intermetallic phase incorporated in the 3A.

2.3.1 PROCESING OF DIFFERENT COMPOSITES USING 3A PROCESS

(a) TiO_2/Al System

After attrition milling of ~1 μm powder of Al and TiO_2, cold pressed samples were heat treated at 1550° C. The formation of $TiAl_3$ leads to the consumption of Al and TiO_2 at temperatures between 500 and 700° C. The formation of titanium aluminides from elemental powders generally starts with the generation of Al-rich phase at Ti-Al interface. Various authors [14,15,62,66,68,70-73] have tried processing of TiO_2 and Al using different compositions. The phases formed depend upon the composition of the powders selected. The formation of the equilibrium phase α_2-Ti_3Al cannot be observed below 1000^0 C. Feng and Froyen [70] studied the starting material 83.33 wt %Al-16.67 wt % TiO_2 up to 1100° C at 10° C /min, Al_3Ti and α-Al_2O_3 are finally formed in the aluminum matrix. TiO and γ-Al_2O_3 were the transition phases during the reactive process. Gaus et al [15,66] determined four critical values of Al/TiO_2 ratios. They studied at a heating rate of 30°C/ min with a hold of 10 minutes at the desired temperature. The four critical ratios were 4.33:1, 2.33:1, 1.66:1, and 0.33:1 for getting $TiAl_3$, TiAl, Ti_3Al and

Ti_2O_3 respectively. However, there is no clear evidence that TiAl is formed with 2.33:1 composition. Schicker et al [69] identified, the Al-rich aluminide $TiAl_3$ as an intermediate product before the stable phase Ti_3Al is formed. One can see from the above results that the Al/TiO_2 ratio should be smaller to get the titanium rich aluminides. The formation of γ-Al_2O_3 resulting from the aluminothermic reaction was observed in the temperature range between 600 and 700° C. Above 1000° C, α-Al_2O_3 transformed to γ-Al_2O_3. It was found that, in the precursor systems with TiO_2/Al ratios of (45/55)(35/65), exhibit relatively low reaction enthalpies. Reaction velocity and maximum heat during reaction synthesis in the temperature range between 550 and 700^0 C, can be easily controlled by using heating rates < 3 K/min. Otherwise (> 3 K/min) due to the highly exothermic character of these reactions, it can result in the formation of liquid phase causing large pores, which cannot be eliminated during pressureless sintering. Fahrenholtz et al [71] observed that the reaction of aluminum and TiO_2 proceeds to completion at 1400° C in argon atmosphere.

(b) Nb_2O_5/Al system

In Nb_2O_5/Nb–Al system, formation of $NbAl_3$ was observed as low as 600°C. After sintering at 1550° C, the samples mainly consisted of $NbAl_3$ and Al_2O_3 [64,65]. Composites prepared by pressureless sintering of compacts made of attrition milled Al_2O_3, Nb and aluminum powder mixtures. The final composite microstructure consists of Al_2O_3, Nb, NbO, $AlNb_3$, and $AlNb_2$ phases. These were typically <150μm size. Amount of initially added Al influenced the formation of the intermetallic phases. Heating rate plays very vital role in this process. Too rapid heating rates gave a loss of process control and the reaction does not occur locally anymore but produces a considerable amount of molten aluminum. Garcia et al [74] used a heating rate of 1°C/ min got dense composites after sintering. Using a heating rate of 3° C /min resulted in a considerable increase in porosity in the sintered samples.

(c) FeO/Al system

In Fe-Al System, it is very difficult to control the reaction between Fe_2O_3 and Al. Since it is highly exothermic reaction, a considerable amount of inert Al_2O_3 must be

added to the starting mixture in order to limit the maximum temperature increase within the sample. It is advisable to add inert phase externally to the systems having high enthalpy of reaction. The enthalpy of reactions of systems of interest is shown in the ***Table 2.2***. The aluminide formation from mixers containing elemental Fe, Al, Al_2O_3 gives early formation of intermetallic phase FeAl at 600°C. After sintering at 1500° C, 3A material results with FeAl and Al_2O_3 as major phases.

(d) NiO/Al system

It has been proposed by Fahrenholtz et al [71] that the reaction between aluminum and NiO be

$$(2+3x) + 3NiO \rightarrow Al_2O_3 + 3NiAl_x \qquad (2.4)$$

where x represents the molar ratio of Al to nickel in the reaction products. Powders of aluminum and NiO (nickel oxide) were mixed in the molar ratio (x=0, x=1/3 or x=1). The ratio of nickel oxide and aluminum produced alumina and either nickel or NiAl after heat treatment at 1673 K. But the x=1/3 did not form Ni_3Al as anticipated. Some residual nickel aluminate remained for each of the reaction. In order to form Ni_3Al above 1127 K, either a catalyst or a secondary heat treatment would be required since formation Ni_3Al is energetically not favourable[71] above 1127 K. But in another study by Zhu and Abbaschian, it was found that different intermediate phases[77-79] were formed depending on the temperatures, Ni formed first at around 600°C, followed by $NiAl_3$, Ni_2Al_3 and NiAl as temperature increased. The formation of Al_2O_3 phases during reactive hot pressing was a three stage process. Initially, a small amount of Al_2O_3 was produced by the reduction of the NiO with solid aluminum. As temperature increases Al_2O_3 particles forms by the reduction of NiO and liquid aluminum. Finally, a $NiO/Ni/Al_2O_3/Ni_xAl_y$ layer structure forms via solid state displacement reaction between NiO and nickel aluminides ($NiAl_3$, Ni_2Al_3, NiAl) leading to the formation of interpenetrating Al_2O_3 network in the final product. Final phases formed depend on the initial composition of the powder mixtures and also on the temperature of the processing.

(e) ZrO_2/Al system

In Al-Zr system, at temperatures <660°C, aluminum reacts with ZrO_2 to form $ZrAl_3$. At temperatures higher than 1000° C, Al_2O_3 and the aluminides sinter together to give dense, porous free composite. A significant increase of net shrinkage and reduction of total porosity (4 vol%,average pore size 3 μm) was observed when the heating rate was raised from 15 to 30° C/min. It has been observed that there were no significant changes in the composition between 25° C and 500° C. At 600° C, peaks related to the formation of the aluminide phase appeared, and the aluminum peaks weakened.The reaction completed at 700° C, the aluminum peaks were replaced by $ZrAl_3$ peaks.The reaction of aluminum with zirconia can be written

$$13\ Al + 3\ ZrO_2 \rightarrow 3ZrAl_3 + 2\ Al_2O_3 \qquad (2.5)$$

with increasing amount of ZrO_2 in the mixture on further heating, the formation of $ZrAl_2$ was observed following the equation

$$10\ ZrAl_3 + 3\ ZrO_2 \rightarrow 13ZrAl_2 + 2\ Al_2O_3 \qquad (2.6)$$

2.3.2 DENSIFICATION BEHAVIOUR

In 45 vol % TiO_2 and 55 vol % Al precursors, between room temperature and 300° C slight expansion and between 450 and 700° C, a linear shrinkage of about 1% was observed ***(Fig 2.3)***. Above 1200° C, the 3A composite starts to sinter. Complete densification with an overall linear shrinkage of 13 % was achieved after 30 minutes at 1550° C. In case of Nb-Al system, in the temperature range of 400° C to 600° C, the sample contracted ~ 2%, and the overall linear shrinkage was 11%. In case of Fe-Al system, up to 580° C samples expanded. At temperatures around 1200°C, samples begin to sinter but while low aluminum (16.8 vol%Al) samples nearly densified with an overall linear shrinkage of 15%. On the contrary, the final shrinkage observed for high aluminum (29.2 vol% Al) is only 5%. Low densification of high Al demonstrated that large amounts of liquid phase have a detrimental effect on the sintering behavior of $FeAl/Al_2O_3$

composites. In Al-Zr system, thermal expansion (~0.5%) up to 300°C took place. Then contracted ~ 1.2% between 400-600°C due to the formation of zirconium aluminides and crystallization of amorphous alumina. The overall linear shrinkage during reaction sintering was about 8%. The use of nitrogen and argon caused lower net shrinkages resulting in lower final densities. Vacuum sintered samples densified better than the sample sintered in inert atmosphere.

2.3.3 MICROSTRUCTURAL DEVELOPMENT IN 3A COMPOSITES

Microstructure of 3A composites can be tailored in a wide range. Principally there are 3 sources of alumina in any of the 3A process (a) admixed alumina powder, (b) alumina resulted from Al oxidation during milling and (c) alumina from redox reaction. Adjusting the green composition using these principles, the final metal/ceramic ratio can be varied between 5 and 60 vol % aluminide. Claussen et al [73] observed that the metal ceramic ratio of 45 Vol% Al – 35 Vol % Al_2O_3 – 20 Vol % TiO_2 gives about 35 Vol % aluminide and typical phase dimensions are about 3μm. The metal ceramic ratio of 45 Vol % Al – 55 Vol % TiO_2 yields about 50 Vol % and the microstructural scale is about 30μm. Externally added Al_2O_3 in the former alloy actes as nuclei for the newly forming phases. So, is the fine microstructural scale (3μm). Schicker et al [75] observed, the sample of composition 16.8Al - 65.1Al_2O_3 - 18.1Fe Vol.%. Microstructure consisted of ~30 Vol.% of FeAl of size about 1-5μm and some residual pores not larger than 3μm. Claussen et al [73] achieved a microstructure of 3μm with a composition of the sample 13.1Vol.%Al, 64.8 Vol.% Al_2O_3, 22.1 Vol.% Fe. In Al-Zr system, the microstructure observed was fine grained. Higher heating rate (>30^0 C/min) led to increased residual porosity. The aluminide/Al_2O_3 interfaces were well bonded and no interfacial failures were observed [75,80]. The ceramic matrix is 1-2μm in grain size and fairly equiaxed.

2.3.4 PROPERTIES

Observed bending strength of 45 Vol. % TiO_2 – 55 Vol. % Al was 420± 32 MPa, and a Vickers hardness of 16.5 GPa at 100 N for holding time of 10 seconds. A room

temperature bending strength of 445 MPa and a hardness of 14.6 ± 0.2 GPa was observed in Nb-Al system. It has been reported that further improvement in mechanical properties may be expected with optimization of milling process and process parameters e.g. green density, initial composition and heating cycle optimization. Mechanical behavior depends strongly on the processing conditions. Bending strengths of 570 MPa have been obtained in the system 16.5 Vol.%Al, 64.8 Vol.% Al_2O_3, 22.1 Vol% Fe and a VHN of 5.7 GPa. Maximum bending strengths of 700 MPa were obtained with 7.4 Vol.%Al, 22.6 Vol.% Fe, 70 Vol.%Al_2O_3, indicating a strong toughening potential by crack bridging of the Fe ligaments. Room temperature flexural strength of 45 Vol.% Al – 20 Vol.% ZrO_2 and 35 Vol.% Al_2O_3 composite was 410 MPa. Properties of different systems are shown in ***Table 2.4.***

During 3A process powders are mechanically milled then compacted and finally sintered in vacuum. During sintering, the oxide powders (Me_aO_b) are reduced to their nascent metallic form and these metallic forms further react with aluminium to form respective aluminides. These reactions are somewhat similar to mechanically milled powders. Both the powders exhibit high reactivity and the reacting mechanisms are likely to be the same. The only difference is, mechanically milled powder undergo microstructural changes due to mechanical alloying (e.g. amorphization). But in 3A process, amorphization part is almost negligible. It is only reaction between two metallic phases (i.e after reduction of the oxide phase) often aluminium is present in liquid form. The phase stability and phase formation in mechanically alloyed powders (especially during sintering) are likely to be somewhat similar to 3A process, once the oxides are reduced to native metallic form. The mechanically alloying results are very useful in analyzing some of the phases that form during 3A process. Hence the mechanisms of mechanically alloyed powder are briefly reviewed here.

2.4 Microstructural development during Mechanical Milling/Alloying

The mechanically driven chemical reduction process (mechano synthesis) has a number of advantages over the commercial metal processing techniques. It enables the

reduction of metal oxides (and halides) directly to pure metals or alloys without first having to convert the oxides to pure metals and then to the desired alloy. For P/M applications it allows the direct formation of a powder product without first having to manufacture the bulk alloy and then convert it to the powder form. In addition to powder cost savings that may arise from the reduced number of processing steps required, additional benefits accrue because the reactions occur at room temperature. Mechanical alloying is a solid state powder processing technique involving repeated welding, fracturing and rewelding of particles in a high energy ball mill. Mechanical alloying is capable of synthesizing a variety of equilibrium and non-equilibrium alloy phases starting from blended elemental or prealloyed powders. The non-equilibrium phases synthesized include supersaturated solid solutions, metastable, crystalline and quasicrystalline phases, nanostructures and amorphous alloys [81,82]. Disordering of ordered intermetallics and mechanical synthesis of materials could also be done by mechanical alloying method. Mechanical alloying (MA) is a high energy ball milling technique, in which elemental blends are milled to achieve alloying at the atomic level. In addition to elemental blends, pre-alloyed powders and ceramics, such as oxides, nitrides etc., can also be used to produce alloys and composites by this technique [81,82]. However, mechanically activated self-propagating high temperature synthesis (MASHS), which is based on a combination of mechanical alloying (MA) and self-propagating high temperature synthesis (SHS). In this process, the powder mixture is mechanically alloyed to produce a nanocrystalline structure and then the SHS reaction initiated by pressing the powder into a pellet and igniting it in a furnace. The prior mechanical alloying step decreases the ignition temperature by as much as 100°C [11]. Several iron aluminide, niobium aluminide and Mo silicide intermetallics were synthesized by this method [11-13,29].

The titanium aluminide alloys can be fabricated by conventional casting and ingot metallurgy techniques. However, the processing costs tend to be high due to a high degree of segregation that occurs during solidification. In casting, section size is fairly limited and specialized techniques like hot isostatic pressing is needed to close the shrinkage porosity. Ingot processing requires multiple treatments to minimize segregation effects and yields tend to be low because of inherently poor workability. P/M technology

eliminates the needs to homogenize ingot segregation [82]. P/M also has the capability to reduce many processing steps through mechanical alloying/milling and followed by hot pressing and heat treatment. This is one of the primary reasons why the TiO_2-Al powders are first mechanically milled followed by hot pressing and heat treatment in the present work.

2.4.1 PROCESSING OF INTERMETALLICS USING MECHANICAL ALLOYING

The ordered nature of intermetallics leads to attractive elevated temperature properties such as high strength, increased stiffness, and excellent oxidation/ corrosion resistance. These attributes are a result of the reduced dislocation motion (since pairs of dislocations, namely superdislocations need to move together to retain the ordered nature of the lattice) and low diffusivities. Also, associated with the reduced dislocation activity is the low ambient temperature ductility and fracture toughness, which restricted large scale industrial applications of intermetallics. Hence, several attempts have been made in recent years to overcome this problem. The common routes adopted to improve the room temperature ductility of intermetallics are: (i) reduction in grain size, (ii) disordering of the lattice, to improve the dislocation motion and (iii) modifying the crystal structure of the phase into a more symmetric. e.g. cubic one. MA can achieve all the above effects simultaneously and therefore, this processing step is an extremely important step to synthesize intermetallics. The types of intermetalics synthesized by MA include quasicrystalline, crystalline, disordered and ordered phases. MA produces almost all the stable and metastable structures produced by rapid solidification processing (RSP). In addition, extended solid solution and amorphous phase formation in the case of liquid immiscible systems have been observed by MA which are difficult to obtain by RSP, making the MA process superior to RSP in many aspects. High energy ball milling has also been used for the production of various intermetallics and nanocomposites by *in situ* reaction, by milling metallic powders in a reactive atmosphere [82].

The actual process of mechanical alloying starts with the mixing of the powders in the right proportion and loading the powder mix into the mill along with the grinding

medium. This mix is then milled for the desired length of time until a steady state is reached where every powder particle reaches to the same proportion of elements in the powder mix. The milled powder is then consolidated in to bulk shape and heat treated to obtain the desired microstructure and properties. Thus, the important components of the mechanical alloying process are the raw materials, the mill and process variables. Process variables to be optimized to achieve the desired product phase and/or microstructure are : type of mill, milling container, milling speed, milling time, ball to powder weight ratio, extent of the milling vial, milling atmosphere, process control agent, temperature of milling and type, size and size distribution of the grinding medium. Intuitively, all these process variables are not completely independent.

Effect of process variables, mechanisms of alloying, characterization of powder after milling, temperature raise during milling, solid solubility extensions were discussed by suryanarayana [82]. Quasicrystalline phases are metallic phases, which exhibit the traditionally forbidden transnational symmetries. These phases have noncrystallographic rotational symmetries, e.g. 5 fold, 7 fold, 10 fold, etc and quasi periodic rotational order. Nature of the phase synthesized was different depending upon the intensity of milling. Soft milling conditions favored the formation of metastable phases both amorphous and quasicrystalline [12,13]. Amorphous phase is furthest from equilibrium while the quasicrystalline phase is intermediate in departure from equilibrium between an amorphous phase and an equilibrium crystalline phase. Amorphous phases have also been reported to occur on milling the quasicrystalline phases. There is also report of formation of a quasicrystalline phase on annealing an amorphous phase [83,84].

A number of crystalline phases have been synthesized by mechanical alloying starting from blended elemental powders [12,78,85-91]. In some cases, formation of intermetallics seems to have taken place by a combustion reaction. Among these cases, there are examples where the combustion took place only after interrupted milling, and then resuming the operation. These results compare very favorably with those obtained in the SHS or combustion synthesis [12,13]. Both ordered and disordered intermetallics have been synthesized by mechanical alloying. In some cases, the intermetallics were

synthesized directly by mechanical alloying; but in others, an additional heat treatment was required after mechanical alloying to form the intermetallic. Since these processing principles are also applicable to 3A process, phases formed by mechanical alloying are both equilibrium and nonequilibrium as mentioned before. The Ti-Al phase diagram features four intermetallics, viz., Ti_3Al (α_2), TiAl (γ),$TiAl_2$ (δ),$TiAl_3$ (***Fig 2.4***) .

The Ti_3Al phase undergoes a disorder-order transformation in the range of 22 to 39(at%) Al and congruently at 1180° C. The ordered α_2 has a hexagonal structure with a=0.5782 nm and c=0.4629 nm. The TiAl phase stable from 49 to 66% Al is considered to be ordered up to the melting point. The γ phase has an ordered face centered tetragonal structure with a =0.4005 nm and c=0.4070 nm and a tetragonality of only 1.02 at the equiatomic position which increases to 1.03 at higher Al contents. $TiAl_3$ is a stoichiometric compound with $L1_2$ type structure ($TiAl_3$ has better corrosion resistance than γ and α_2, since more aluminum content. But it is brittle than γ and α_2 because of low-symmetry structure).

All these intermetallics are lightweight, have high specific strengths, high elastic moduli, good corrosion resistance, and retain sufficient strength up to elevated temperatures. The two titanium rich aluminides (α_2 and γ), are attractive candidate materials for potential applications in advanced aerospace engine and airframe components [82, 92-95]. High-energy ball milling is employed to fabricate this alloy. During mechanical milling several metastable transitions occurred. Alloy consolidated with metastable FCC powder has a much higher strength and better fracture toughness than the cast $Al_{67}Mn_8Ti_{24}Nb_1$ alloy and the monolithic $L1_2$ type Al_3Ti alloys [96]. The materials consolidated consist of fine grains and improved the fracture toughness. This is attributed due to crack deflection and bridging effects of the second phase particles combined with the very fine grains in the alloy. There has been lot of activity in utilizing the technique of mechanical alloying to synthesize these intermetallics to produce them in a nonocrystalline and disordered state to improve their ductility. Even though actual improvement in ductility is yet to be realized in mechanically alloyed nanostructured

titanium aluminides, lot of information is generated on the phase evolution in these alloys [81,82]. Suryanarayana [82] identified the phase formation sequence using XRD patterns.

β Ti + Al → Ti (Al) solid solution → amorphous phase → FCC(contaminant) phase.

If the milling were to be stopped at the correct time, the powder would not get seriously contaminated, and one can end up with either a solid solution or an amorphous phase. Proper precautions have to be taken when reactive metal like titanium is being milled. Investigations on the Ti-Al system, it has been reported that either a supersaturated solid solution or an amorphous phase is formed on mechanical alloying. But α_2 and γ phases could not be synthesized by mechanical milling [82]. The desired intermetallics could be obtained in the appropriate composition range, only after a suitable heat treatment. For example, annealing of the mechanically alloyed Ti-24 at% Al powder for four weeks at 903 K produced the α_2 -Ti_3Al phase [86]. Similarly, the γ phase could be produced only after annealing the as milled amorphous powder of appropriate composition for 168 hours at 888 K [82]. These temperature and time could vary considerably depending on the powder particle/grain size. However, the Al_3Ti phase could be synthesized in a metastable $L1_2$ structure directly by mechanical alloying [97]. Systematic studies on the transformation behavior of metastable phases to the equilibrium phases have not been undertaken in mechanical alloyed powders. The transformation behavior of the $L1_2$ type Al_3Ti phase produced in Al-25Ti alloys was studied by annealing the powders at different atmospheres. The as-milled powder contained the $L1_2$ and Al (Ti) solid solution phases. Annealing of these two phase structure at 673 K for 1 hour at temperatures > 1073 K [97]. Considerable amount of literature also exists on the synthesis of Nickel and Iron aluminides, Mo silicides and Ni-Ti intermetallics[98-113]. The interesting observation is that the equiatomic NiAl phase is produced via a combustion synthesis [12]. Combustion synthesis took place only after interrupted milling, i.e. milling of the powders for a given length of time, aging the powders at room temperature after stopping the milling, and then resuming the milling operation. For example, in the Al-Ni system, an intimate mixture of aluminum and nickel phases was detected after milling the blended elemental Al-Ni mixture for 2 hours. If the milling is stopped and the powder is stored at room

temperature for 30 minutes, and then milling is resumed, it is noted that the NiAl phase formed just after 1 minute of milling due to the occurrence of an explosive reaction [98]. Similar reactions were also observed in the synthesis of $MoSi_2$. It has also been reported in some cases that intermixing among the powder particles takes place continuously and metastable phases form prior to the formation of the equilibrium phases. The times required to form a particular phase depend on the initial concentration of solute in the powder mixture. If the solute content were much less than the exact stiochiometry, the expected phase (although the proportion of phase in the mixture of phases is less) would form at much longer milling times. Even though the intermetallics synthesized by mechanical alloying include both the ordered and disordered types, it is not surprising that mechanical alloying produces disordered phases. This is because mechanical alloying involves heavy deformation and it is known to destroy long range ordering in the lattice [12]. A large number of intermetallics have been synthesized. Some of the interested systems are shown in ***Table 2.4***.

Reasons for formation of intermetallics have not been investigated in detail. It may be assumed that a phase will exist either in the ordered or disordered condition depending upon the balance between atomic disordering introduced by mechanical alloying and the thermally activated reordering. The reordering is caused by the difference in energy between ordered and disordered states. Thus if this difference in energy is small, the alloy will exist in the disordered state and where as if it large the alloy will be in the ordered state [99]. The same argument can be extended to the Ti-Al system.

2.4.2 SOLID STATE AMORPHISATION DURING MECHANICAL ALLOYING

A solid alloy with a liquid like (non crystalline) atomic arrangement is called a metallic glass. Solid state amorphisation (amorphising a solid with out passing through the liquid state at any stage) reactions include irradiation, hydrogen assisted amorphisation, interdiffusion of elemental metals, pressure induced vitrification, and

mechanical deformation. Recently, amorphous phases have also been synthesized by mechanical alloying or mechanical milling starting from : (a) Blended elemental powder mixtures, (b) prealloyed powders and/or intermetallics, (c) mixture of intermetallics and (d) mixture of intermetallics and elemental powders. ***Table 2.5*** shows the phases formed based on the milling conditions. One can see the variety of phases that can be achieved by MA/MM.

It is clear from the ***Table 2.5*** that amorphous phases can be formed by various stiochiometric compositions of Ti-Al and with alloying elements of various compositions. The amorphous phase formation is known to be critically dependent on the milling conditions. Details about the mill, milling container, grinding medium, balls to mill ratio (BPR), and other parameters are provided in the ***Table 2.5***. Amorphous phase forms by mechanical alloying from a mixture of powders (A and B) and by mechanical milling from the intermetallic compound (A_mB_n). When the starting material is a mixture of elemental powders form, it takes longer time for amorphization. On the other hand, when starting material is a stoichiometric intermetallic powder, amorphization takes place in a short span of time. In some of the systems, prior to amorphization, some crystalline phases or solid solutions may form [12,82]. Amorphisation in ordered Al-Ti alloys seems to follow the following sequence.
Ordered phase→ disordered phase (loss of long range order) → fine grained (nanocrystalline) phase → amorphous phase.

2.5 Mechanical alloying, microstructure and properties of Ti-Al systems

2.5.1 MECHANICAL ALLOYING

Some 300 intermetallic compounds with high melting temperatures are candidate materials for the high temperature turbines and engines of the future. These intermetallics have superior modulus to specific gravity ratio. The specific strength of TiAl alloy

exceeds that of the common titanium alloys and matches to some of the nickel base alloys (*Table 2.6*).

Particle shape and size influence compaction of green powders. As we have seen earlier, mixing and compaction of green powder play an important role in combustion synthesis reaction. In addition, heating rate is also an important parameter for getting the final product. Yi et al [86] studied the Ti-Al reaction system using different reaction stoichiometries and found that there were two exothermic peaks during the reaction. The first exothermic peak occurred only when the heating rate was low (< 2 K/min). The heating rate also affected the density of the products in the formation of $TiAl_3$. It was found that the relative product density increased from ~29 to ~55 % as heating rate changed from 2 to 50 K/min.

Several authors prepared titanium aluminides, Mo silicides, iron aluminides, Nb aluminides and Ni-Ti (shape memory alloys) intermetallics using MA followed by suitable treatment [34-39]. For example, Mukhopadhyay et al [47] synthesized $TiAl_3$, TiAl, Ti_3Al intermetallic compounds by MA of $TiH_{1.924}$ and aluminum powders, followed by annealing. Ward-Close et al [48] studied two methods of controlling the grain size in gamma TiAl type alloys using mechanical alloying and HIPing. In one method, selective MA of the surface region of powder particles occurs, while in the other a mixture of unmilled and MA powder were blended together. In both cases the HIPed material consisted of mixed small and large grain sizes. In other attempt, Rao and Du [49] prepared Ti_5Si_3/ TiAl *in situ* composites. TiSiAl based metastable precursors were first synthesized by MA, and blended with Ti-50Al powder matrix. The composite was first pressed to pellets followed by heat treatment to initiate reactive sintering that led to the formation of Ti_5Si_3/ TiAl composites. A phase hierarchy has been observed during *in situ* formation of the reinforcement, i.e.,

$$TiSi_2 \rightarrow Ti_4Si_4 \rightarrow Ti_5Si_3 \qquad (2.6)$$

However, Orru et al [50] synthesized titanium aluminides (Ti_3Al and TiAl) through field activated SHS. At sufficiently high field, a single phase product was obtained in the case of Ti_3Al. But in the case of TiAl, the product contained Ti_3Al as a secondary phase even with the highest imposed field. The results show that the synthesis by SHS can be optimized by the combination of field strength and relative density. To prepare the mechanically alloyed powders for SHS reaction, mechanical alloying time should be optimized because too short length of mechanical alloying decreases the heat of reaction due to the formation of Al supersaturated solid solution during mechanical alloying [51]. Similarly, in case of Fe-Al, Nb-Al and Ni-Ti the microstructure scale obtained was nanostructure after MM followed by annealing. In all of these cases green density played vital role in achieving final product density and microstructure.

In the recently emerging class of gamma Ti (46-48)-Al based alloys with about 2% additions of Nb and about 2% of some other elements (e.g.Cr, Mn, W, Ta, Si, B), tensile ductilities as high as 4% were achieved at room temperature [52]. However, microstructures with acceptable ductilities often show poor toughness (K_{Ic} ~10 MPa$\sqrt{m}$) and reduced creep strength where as microstructures with both improved toughness (~30 MPa$\sqrt{m}$) and creep strength led to unsatisfactory ductilities. This inverse correlation between tensile properties and resistance to fracture renders microstructural optimization for achieving balanced engineering properties to be very difficult and some more work is needed in this direction. A minimum amount of boron (~0.5 at%) is required to refine the grain size [53-57]. Below this level little or no impact on the grain size was observed where as adding larger amount of boron did not reduce the grain size further. In some cases, boride particles are invariably observed as B solubility in TiAl is very low.

2.5.2 Microstructure and properties of different Ti_3Al and TiAl alloys

Microstructure control can be achieved by an optimum combination of alloying and processing. Generally transformed β microstructures (to produce elongated plate like α_2) have been considered to be the best microstructure because this structure was considered necessary to achieve the best balance of room-temperature ductility and elevated temperature properties. More recently, equiaxed α_2 morphologies have been

investigated because of their potential for increased room temperature ductility [114-117]. A small α_2 grain size increased strength; and generally a refined slip length improves ductility levels, using either grain size, the allotropic change, or precipitation of second phase particles [116,118-124].

The fracture behavior in these alloys is related to slip behavior in the α_2 phase and also to the presence of the β/B2 phase. The tensile properties of Ti_3Al-Nb alloys are critically dependent on the shape, distribution and volume fraction of the α_2 and B2 phases [114], with boundary strengthening playing a dominant role [21,22]. Widmannstatten secondary α_2 resulted in better ductility than microstructures with an aligned α_2 morphology, with aligned colonies acting as single units. Increasing the final α_2 volume fraction (up to 30%) in a fine widmannstatten microstructure in the Ti-25Al-10Nb-3V-1Mo alloy decreased the yield strength of the alloy due to decrease in volume fraction of fine matrix. The ductility depends on both the distribution and volume fraction of the α_2 phase and peaks at 30-35% α_2, a trend which was attributed to the cracks which formed in the relatively large primary α_2. This behavior apparently does not parallel that in conventional titanium alloys in which increasing the amount of equiaxed primary α enhances ductility. However, it was clearly shown that if an optimum amount of equiaxed α_2 grains are produced by thermomechanical processing, room temperature ductility could be dramatically improved (to 26% elongation), removing the inconsistency with the behavior of conventional titanium alloys. Grain boundary α_2 allows easy crack propagation and increases strain incompatibility at the boundary. In Ti-24Al-11Nb alloy, the maximum elongation, of close to 10% in α_2+β processed material occurred at 30-35 Vol. % of the α_2 phase. Interestingly, this corresponds to the maximum in yield strength for fine α_2 plates with primary α_2 present. α_2+β processed material exhibited higher densities than β processed material. It was suggested that the easy cracking in the primary α_2 regions dominated with some evidence of cracking along α_2-β interfaces; however, microcrack propagation across adjacent transformed β regions was difficult. Optimum creep behavior was suggested to be associated with a basket weave α_2 microstructure with a minimum of β phase. The finer scale microstructure obtained when stiochiometric

α_2 is alloyed with β stabilizers such as Nb, V, or Mo, in combination with β regions forming a continuous layer surrounding α_2 grains, enhances the ductility [94,117,125,126]. However more work is required to fully optimize the microstructure for a combination of mechanical properties; the high ductility (26% room temperature elongation) emphasizing this point.

The mechanical properties of monolithic α_2 alloys depend on composition and the microstructure developed by thermomechanical processing. The composition evaluated span 0-30 equivalent Nb content with the majority of the mechanical properties improving with increased Nb content. However, increase in Nb content may reduce creep resistance. But richer Nb containing alloys contain the orthorhombic phase, may be useful for high temperature applications. Typical mechanical properties of α_2 alloys are listed in ***Table 2.7***. Two phase alloys exhibiting up to a doubling of strength due to predominantly to boundary strengthening, with long range order, solid solution and texture effects also contributing. However, the mechanism by which the ductility of α_2 alloys improving with the addition of Nb is not clear till today. Increasing the Al level and the amount of β stabilizers both resulted in increased yield strength. A fine widmannstatten structure with a small amount of primary α_2 grains exhibits better ductility than microstructures with a coarse widmannstatten microstructure or an aligned acicular α_2 morphology.

Fatigue properties of titanium alloys are strongly influenced by microstructure. The low ductility exhibiting in material with widmannstatten α plates in $\alpha+\beta$ alloys is responsible for low elevated temperatures LCF strength. Fracture toughness appears to depend on microstructure as well as alloy composition but the precise relationship is yet to be defined [94,125-139]. The decrease in toughness of the Ti-25Al-10Nb-3V-1Mo alloy may result from an increase in the Mo level in conjunction with a higher strength level. The higher (17 At%) Nb level appears to have the capability of combining toughness with strength and creep behavior. The Ti-15 Al-22.5 Nb alloy has the highest fracture toughness reported for a α_2 type alloy but the creep rupture resistance is

extremely low. Charpy impact strength levels of the titanium aluminides (2-3 J compared to ~25 J for conventional titanium alloys) are a major cause for concern in application like turbine blades. Mechanical properties and creep properties of various combinations of alloying elements of α_2 are summarized in ***Table 2.7.***

Microstructure effects on creep can be as significant as compositional variation. Although compositional effects are not yet clear, the microstructure/creep behavior of Ti-25Al-10Nb-3V-1Mo has shown that the colony type microstructure is characterized by enhanced creep resistance over other microstructure. The creep resistance of Ti-25Al-10 Nb-3V-1Mo is raised by a factor of 10 over conventional titanium alloy Ti-110 and two orders of magnitude over Ti-6 Al-2-Sn-4Zr-Si. The elements like Si, Zr appears to improve creep resistance but the most significant increase attained by increasing the Al content to 25% and limiting β stabilizing elements to about 12%. Ti-26Al-5Nb indicated that addition of Nb decreased the creep resistance. Ti-24Al-11 Nb alloy, study of the stress dependence of the steady state creep rate, shown that the microstructure with a coarse α_2 lath size, in general, display improve creep resistance over fine lathed structure [140]. The nature of the complex α_2/α_2 or α_2/β interface structure may significantly influence the mobility of dislocation and thus creep rate.

The microstructure of the γ alloys can be single phase γ or, in slightly leaner compositions, two phase $\gamma+\alpha_2$. Further, by appropriate thermomechanical processing, the morphology of the phases can be adjusted to the either lamellar or equiaxed or a mixture of both morphologies [114,118,131,132]. The lamellar structure can lead to an effective refinement of the microstructure and improved ductility either directly or in combination with fine recrystallized γ grains [120,134]. Improved ductility occurs at about 10 vol% α_2; when α_2 phase content exceeds 20 vol % ductility decreased. This is consistent with the fact that α_2 becomes increasingly more brittle with increasing aluminum content over 25 % and the α_2 plates have a composition of approximately 35% Al. In dual phase alloys, the ratio of lamellar to equiaxed γ must also be controlled along with their distribution. A lamellar volume fraction of about 30 % gives a reasonable combination of properties with good high temperature creep resistance and acceptable tensile strength

and usable ductility. The optimum structure for enhanced ductility has been suggested to consist of adjacent regions of lamellar and equiaxed morphologies. The grain size decreases with additions of W, V, Mn, and Cr [121,131,134,135]. The number of annealing twins in the γ phase increases as aluminum content decreases or when Mn or V levels are increased, while Cr additions increase the volume fraction of the lamellar structure. Materials with an extremely small (nonostructure sized) grain structure have exhibited high room temperature elongation up to 5%, clearly an area of worth studying.

The most effective method of microstructure control for γ based alloys will be thermomechanical processing of ternary or quaternary alloys to produce a duplex structure based on γ+ α_2 or β [131]. Dispersion of phases such as TiB_2 or Er_2O_3 is reported to be effective for strengthening of the matrix. TiAl based alloys are generally two phase, it has been shown that by manipulating the microstructure at room temperature ductility can be 2%, which is apparently acceptable to design engineers. Thus the alloys based on TiAl are commonly produced either as lamellar structured alloys, where TiAl and Ti_3Al make up the lamellae (a duplex structure) and the grains of TiAl are interspersed with some lamellar regions. The duplex alloys are generally (but not always) somewhat weaker than the corresponding lamellar alloys but show better ductility and clearly the choice of the structure will be different for different potential applications. When lamellae were inclined to the stress axis, the flow stress is low and elongation is high. If the stress is applied either parallel or perpendicular to the (0001) interfaces of lamellae, then elongation is small and flow stress is high. It has been observed by Saqib et al [136] that the TiB_2 particles are found to be very effective in refining the grain size of the Ti- 43 Al alloy. No detectable change observed in the size or the number density of the TiB_2 particles due to the Oswald ripening, and the particles were virtually stable at temperatures up to 1473K [136, 137].

The ductility of the Ti-50 Al alloy was considerably increased by decreasing the initial grain size to 5 μm so that even at 700°C, the specimens were deformed to a strain of 80% without fracture [138]. Imayev et al [132] observed that in Ti_3Al a critical grain size, d_{cr}, exists below which the intermetallic in the ordered state begins to exhibit

noticeable ductility. This critical grain size increases as the temperature increases. For example, d_{cr} is equal to 0.8 μm at room temperature, 5.5 μm at 300° C and 27 μm at 400° C. So, the selection of initial powder sizes is a very important parameter to get reasonable ductility at room temperature.

At a grain size (TiAl) of 8μm, the transition from deformation by slip to deformation by twinning takes place. So the ductility of intermetallics increased with increasing strain rate for the above grain size [13]. Transition from microcrystalline (d~ 1 μm) to the sub-microcrystalline (d<1μm) grain sizes in TiAl resulted in an abrupt reduction of porosity after superplastic deformation while retaining very similar values of super plastic parameters δ and m [119]. Here δ and m are maximum relative elongation to fracture and strain rate sensitivity coefficient respectively.

The Nb containing alloy (Ti-45Al-10Nb) shows remarkable high tensile strength both at room temperature and 700° C [141]. The tensile properties of this alloy are impressive if the specific strength is considered which up to 750° C exceeds that of high strength superalloys as well as high temperature titanium alloys (see ***Table 2.6***). Strength of niobium alloys contributed to microstructural refinements as a consequence of the reduced aluminum contents. Ti-45Al-10Nb alloy with duplex microstructure, appreciable room temperature ductility has been observed. Further work was planned by the authors to optimise room temperature properties and creep strength. The work also focuses on improving microstructural homogeneity by processing as well to the alloy composition, (in particular alloying elements) which improve microsrtuctural stability and creep resistance. Chromium addition [135] enhanced the plasticity of duplex alloys, but except no ductilisation and the structure is fully transformed α or single phase γ. Increase in plasticity of chromium containing aluminide can be seen from the ***Table 2.8***. The specific strength of TiAl alloy exceeds that of the common titanium alloys and matches some nickel base alloys [142]. Sheets can be produced using ingot metallurgy or powder metallurgy plates. Ingot processing requires a significant amount of thermal mechanical processing to break down and homogenize the ingot microstructure. Even after several forging steps, the microstructure varies locally due to segregation in the original ingot.

With the powder metallurgical process, using gas atomized powder and HIP, a plate with a fine uniform microstructure can be made directly to the dimensions required for rolling. The resulting sheet has a homogeneous microstructure and uniform properties. Laser formed aluminide had a fine microstructure. It was showing better properties as compared to other processes. Fabricating titanium aluminide parts from this process is extremely difficult. Comparison of various properties is shown in the ***Table 2.8.***

Spray formed aluminide achieved room temperature tensile test yielded plastic elongation of about one percent and strength levels of $\sigma_{0.2}$ ~ 400MPa and UTS ~ 470 MPa [140-143]. Future work can be directed for subsequent thermomechanical processing of the resultant deposits. Alloy based on the titanium aluminum (γ) composition have higher elastic modulus, lower density, enhanced elevated temperature capabilities, and are less likely to ignite than Ti_3Al alloys [144,145]. However, room temperature ductility and fracture resistance can only be classed as poor. General trends are for a slight decrease in stiochiometry, into the two phase $\gamma + \alpha_2$ region, to increase ductility. For enhancing ductility small additions of (1-3%) V, Mn and Cr, Nb, Ta, and Mn improving strength and oxidation resistance [121,131,133,134]. Ti-52 Al alloys demonstrates the lowest hardness value at room temperature independent of thermomechanical processing treatment. At 1000°C, the strength tends to gradually decreases with aluminum level . The room temperature tensile elongation is maximum at approximately Ti-48Al. Values of room temperature ductility slightly in excess of 2% elongation is possible with chemistry control (two phase region). Although excursion down to the nanostructure region of the microstructure scale can apparently increase this level up to 5%, and at the same time decrease in DBTT by as much as 200°C. Chan and Kim [125] reviewed toughening mechanisms in two phase titanium aluminide alloys. Both intrinsic and extrinsic toughness mechanisms were present in Ti_3Al alloy and TiAl base alloys. The former affects the initiation toughness at the on set of crack extension, while the later leads to crack growth toughness by instigating resistance curve behavior. Intrinsic toughness arises from matrix slip and ductile phase blunting. Extrinsic toughness arises from crack deflection; ductile phase bridging, shear ligament toughening, microcrack shielding, twin toughening and the growing crack singularity. The control of

microstructure is key thing to achieve desired mechanical properties. The area so far has not been examined in detail is weather or not synergetic toughening effects can be obtained through a combination of toughening mechanisms which might include ductile phase blunting, ductile phase bridging, ligament toughening and twin toughening. It has been observed that the α_2 is ductile when it exits in the form of sub micron size thin plates. Ductility and fracture toughness exhibited by individual colonies of α_2 and γ platelets. However, the source of such improvement is remained unknown and the effects of size scale on these properties are yet to be studied.

The fracture mechanism in the duplex microstructure are plasticity induced grain boundary de-cohesion and cleavage, while those in the lamellar microstructure are interface delamination and cracking across the lamellae. The lamellar microstructure is tougher than the equiaxed γ or duplex microstructure because of higher near-tip plasticity and an anisotropic composite like fracturing characteristic that yields a tortuous crack path; shear ligament toughening and an improved resistance-curve behavior. Tensile ductility of the lamellar microstructure increased with decreased colony size, while fracture toughness was maximum at a large colony size. There was no correlation between fracture toughness and measured tensile ductility in the two-phase TiAl alloy studied by Kim [92]. Annealing in the $\alpha+\gamma$ and /or $\alpha_2+\gamma$ phase fields of the binary Ti-48Al alloy was not significantly affected the fracture toughness. It was observed in the lamellar microstructure that microcracking, crack branching and crack bridging by uncracked ligaments, which enhanced stress-shielding effect in γ-base titanium aluminides. Lamellar microstructure materials exhibited high fracture toughness compared with duplex microstructure materials. Alloying additions affected the fracture toughness at elevated temperatures significantly. The addition of Cr improved the low temperature fracture toughness (below 800°C), while the addition of niobium increased the fracture toughness above 800°C, but how the fracture toughness increased by the addition of Nb and Cr is still not clear. The result of Suboyejo et al. [128] was contradictory that Nb additions decrease the tensile strength and ductility. In general Nb addition increases tensile strength [127]. Low cyclic fatigue experiments suggest that fine grain sizes raise the fatigue life at temperature below 800°C. Fatigue crack growth rates

are more rapid than those for superalloys. Both fracture toughness and impact resistance are low at ambient temperatures, but fracture toughness increases with temperature. Fracture toughness increase with higher portions of lamellar structure [94,114,125-129]. In a two phase quaternary γ alloy a fracture toughness of 12MPa $\sqrt{m}$ is observed for a fine structure which is almost entirely γ and K_{IC} > 20MPa $\sqrt{m}$ (~35) when a large volume fracture of lamellar grains are present.

Creep properties are improved beyond the behavior of superalloys when normalized by density, but are strongly influenced by alloy chemistry and thermomechanical processing (TMP) [114,145-147]. Increased in Al content and additions of W increase creep resistance. In single-phase γ region (Ti-53.4Al at%) there was no influence of grain morphology on creep behavior. However, at leaner Al contents (Ti-50 Al at%), a small amount of second phase was observed along grain boundaries, which enhanced creep behavior. This work suggested that creep in TiAl is not simply diffusion controlled as it is in normal metals. Increasing the volume fraction of the lamellar structure enhances creep properties, but lowers ductility. Ductile brittle Transition temperature (DBTT) took place between 600-700 °C. For Ti-50 At %Al they observed the DBTT in the range of 800-850 °C [121,148]. This is some discrepancy with the literature. Generally, porous micro cracking appeared before failure of specimens. In case of Ti-49 At% Al there is a difference in low temperature and medium temperature behavior.

Hipping of 100-150μm powders produced a fine grain size of about 30μm. Hipping was done at 1200 °C, 200MPa for 2 hours. A fully dense intermatallic γ-TiAl has been produced [149]. However, cold compaction followed by hipping (with out canning) produced with numerous cracks on the surface. The synthesis of TiAl occurs by the melting of Al particles (660°C) and the aluminum liquid spreading on the Ti particles. Subsequently, TiAl is precipitated in an exothermic reaction where the heat of reaction makes the porous self-propagating until completion.

2.6. Approaches for ductilisation of different Ti-Al alloys

Various methods usually adopted to ductilise the intermetallics, its alloys and composites are summarized below.

1. Reduction in grain size (usually grain size <0.8 μm).
2. Disordering of the lattice to improve the dislocation motion (superdislocations do not exist in disordered lattices and therefore only single dislocations need to move for deformation to occur).
3. Modifying the crystal structure of the phase in to a more symmetric, e.g. cubic one.
4. Conventional Chemistry-processing-microstructure approach.

Mechanical alloying [59,81-89,97-99] can achieve first three approaches simultaneously and therefore, this processing technique has been extensively employed to synthesize intermetallics. It has been reported [115-118,132,133,153] that a grain size of roughly 1μm would be the optimum grain size to increase the ductility of intermetallics. Chemistry processing microstructure involves alloy design [52,53,114,155-159], addition of alloying elements, processing and heat treatment (thermo mechanical treatments). Microalloying [52,53,114,130,134,135,148,155-159] involves addition of alloying elements such as Nb, Cr, Mn, W, V, B and H_2 to improve the ductility by altering the chemistry of the phases, grain boundary cohesion, grain refinement etc. For example, the ductility of Ni_3Al was increased from almost 0% to more than 50% by doping with boron. Similarly, TiAl was ductilised to some extent (up to 5-6%) by grain refinement. Processing [39,46,122,158-161] also improves the ductility by grain refinement and microstructure uniformity through thermomechanical treatment.

2.7 Digital Image Processing

Importance of quantitative image analysis in various fields such as material science, biology, geology, mediene, petrography has become increasingly apparent from past thirty years. Some of these applications include quantitative and qualitative analysis of materials, automatic character recognition, industrial machine vision for product assembly and inspection, military recognizance, automatic processing of finger prints,

screening of x-rays and blood samples, and machine processing of aerial and satellite imagery for weather prediction and crop assessment. Stereology can be applied to quantitative and qualitative interpretation and characterization of spatial features of materials [162-164]. Quantitative stereology attempts to characterize numerically the geometrical aspects of the two-dimensional features of the microstructure, then correlates it to three-dimensional features of the material. These microstructural features can be successfully quantified using digital image analysis (DIA) tool. Image processing is based on mathematical morphology to extract image information and to represent it as quantitative values that characterize the microstructure. A digital image is an image $f(x, y)$ that has been discretized both in spatial coordinates and brightness.

Purpose of using DIA is to identify the phases (segmentation of binary image), determinations of volume fraction of the phases, surface area, mean free path and spatial distributions in three-dimensional structure.

Interest in image processing stems from two principal application areas: improvement of pictorial interpretation for human interpretation, and processing of scene data for autonomous machine perception. Image processing consists of Image acquisition, preprocessing, segmentation, representation and description, recognition and interpretation which gives the required result. The first step in image analysis after acquiring the binary image is segmenting the image. Segmentation subdivides an image in to its constituent phases in the microstructure. To determine volume fraction and surface area of the aluminide alumina phases, a quantitative characterization of the microstructure using Image Analysis software is performed. Soon after image acquisition, the image has been converted to binary image to perform the measurements. Segmented the binary image by thresholding the histogram in to various phases of interest. Then performed the measurements using area and perimeter of the threshold images for obtaining volume fraction and surface area of phase of interests. Area per area ( ) gives volume per volume (V_v), volume fraction of the phase. Perimeter gives the L_A that can be related to S_v using ($4/\pi . L_A$).

CHAPTER 3:EXPERIMENTAL PROCEDURE

3.1 Introduction

This chapter describes experimental procedures adopted for synthesis and characterization of microstructures of the intermetallic/ceramic (Ti_xAl_y/Al_2O_3) composites. Synthesis consists of mechanical milling, hot pressing and heat treatments. Characterization of microstructures is performed using Optical microscopy, EPMA (Electron Probe Micro Analyzer), XRD (X-Ray Diffraction), SEM (Scanning Electron Microscope), Quantitative microscopy (Image processing). Microstructural characterization is to identify the various phases also their distributions in the composite. Mechanical Property measurements include: flexural strength and fracture toughness using four point bent test and measurement of modulus (*E*). DSC (Differential Scanning Calorimetry) has been performed on selected samples to equilibrium transformation temperature. Microhardness of phases has been performed using Vickers diamond pyramid indentor. Bulk density of the composites is measured using Archimedes principle in water.

3.2 Composite Processing and Characterization

Different powder mixtures used in the present study are summarized in ***Table 3.1***. Powders of aluminum (particle size of d_{50}=33μm, The Metal Powder Company Limited, Madurai, India) and TiO_2 (particle size of d_{50}=20μm, Nano Tek, Burr Ridge, IL, USA) were prepared by ball milling for 8 to 9 hours in acetone using 5mm dia Al_2O_3 balls. Subsequently, dried and thoroughly mixed with mortar and pestle in order to remove agglomerates. Hot pressed samples with dimensions of 12mm dia, using a pressure of 6.4 MPa (Model DPS-6, Dr.Fritcsch K.G., Germany) and 50×25×5 mm^3 (Electro fuel, Canada) were made by uniaxial pressing at 8 Mpa using graphite die and punches (shown in ***Fig. 3.1***) at ~900 to 950° C through resistance heating. Heat treatment (Nabertherm

furnace) of the samples was performed in vacuum (10^{-3}bar) using a heating rate 4°C/min with different holding times at 1400° C.

Phase identification was performed by XRD (Iso-Debyeflex 2002) at each stage of processing (as received powders, blended and milled, hot pressed and heat treated) of the samples. Green samples of 12mm dia were formed by uniaxial pressing at 40 MPa (at room temperature) and heat treated at 1400° C in vacuum for comparison of phase evaluation. Bulk densities of the heat treated were determined using the Archimedes principle in water. Image analysis was done using Image-Pro Plus V.4.1 (Media Cybernetics, L.P, MD, USA). To determine volume fraction and interconnectivity of the aluminide alumina phases, a quantitative characterization of the microstructure using Image Analysis software was performed.

DSC (Differential Scanning Calorimetry) data has been acquired to identify the reaction temperatures of the process. To verify the solid state reaction of the 3A process, DSC was conducted. Using powder mixtures of aluminum and TiO_2 up to 650° C data has been acquired. A constant heating rate of 4°C/min was used between room temperature and 650°C.

3.3 Microstructural characterization

3.3.1 X-RAY DIFFRACTION (XRD)

XRD pattern were obtained using an X-ray diffractometer (Iso-Debyeflex 2002), having a cu target ($K_{\alpha 1}$, λ=1.514 A°) for all the samples. XRD is performed on as received powders, blended and milled powders of different compositions, cold pressed, hot pressed and heat treated samples. About 0.5 g of the powders was used for powder samples to get the diffraction patterns. The settings used for X-ray diffraction are given in ***Table 3.2***. The diffraction pattern was recorded using a software program. Scanning was made from 20 to 80° (2θ) to locate the position of the different peaks.

3.3.2 Optical Microscopy

Samples for microstructural examination were sectioned using a slow speed Isomet saw. Small pellet samples were used directly for microstructural examination. The samples were polished on a series of emery papers. The final polish was done with one-micron diamond, followed by 0.05-micron alumina. An optical microscope (Lietz) was used for preliminary microstructural examination of phases and phase distributions.

3.3.3 Scanning Electron microscopy (SEM)

SEM (JSM 840A, JEOL) was used for fractography of the fractured composites, tested using four point bend test for flectural strength and fracture toughness measurements. Phase behavior observation aroung the indentation using Vickers micro indentor.

3.3.4 Electron Probe Micro Analyzer (EPMA)

EPMA was used to identify the phase's present in the microstructure using point analysis. Also used for mapping of titanium and aluminium distribution in the microstructures. On selected samples, line analysis (diffusion of elements) and qualitative analysis was performed.

3.4 Mechanical Testing

The mechanical tests performed on the composite were microhardness, modulus (E), flexural strength and fracture toughness. The flexural strength and fracture toughness were carried out in an Instron 1195 machine, using a 4-point bending fixture with 10 mm and 26 mm inner and outer spans, respectively. A constant (slowest) crosshead speed of 50μm/min was maintained for all tests until failure occurred.

3.4.1 VICKERS MICROHARDNESS

Microhardness measurements (Leitz, Miniload 2) were carried out to measure the hardness variations in the matrix, as well as reinforcement phase. The test was performed at room temperature by dropping a loaded diamond indentor (60-100g) on different phases. In each case on an average at least 5 readings were taken with a loading time of 10 s.

3.4.2 FLEXURAL STRENGTH

Flexural strength was carried out on a brass 4-point fixture with cylindrical steel pins at the inner and outer span positions. Rectangular beam specimens of 42×3.8×3.8 mm^3 dimensions were cut using an Isomet diamond saw and the surfaces were polished to one-micron finish. Each sample was placed in the fixture as shown in the ***Fig.3.1*** and loaded in an INSTRON 1195 machine. The load vs. displacement data was recorded on a strip chart. The flexural strength was calculated according to the expression [165]

$$\sigma_y = \frac{3P}{bw^2}\left(\frac{d_2 - d_1}{2}\right) \tag{3.1}$$

Where P is the load at the failure, b is the breadth, w is the width of the beam, and $d_1$and d_2 are the inner and outer span lengths, respectively, of the 4-point jig.

3.4.3 FRACTURE TOUGHNESS

For fracture toughness (K_{Ic}) measurements, in addition to the sample preparation for flexural strength, a notch roughly one-third of sample width (w) was introduced mid-span using the Isomet saw. The sample was placed in the four-point flexure as shown in ***Fig.3.1***, such that on loading the notched face would be in tension. The fracture toughness was calculated using the following expression [8, 166]

$$K_{Ic} = \frac{3Pa^{1/2}}{bw^2}\left(\frac{d_2 - d_1}{2}\right)\left[3.86 - 6.15\left(\frac{a}{w}\right) + 27\left(\frac{a}{w}\right)^2\right]^{1/2} \tag{3.2}$$

Where a is the notch depth and other terms are similar to those in the above shown flexural strength equation.

3.4.4 DIGITAL IMAGE PROCESSING

Computers and image processing algorithms provide very powerful tools for the development of automated image analysis system, providing the researcher with the precision he needs to analyze the materials behavior. Digital Image analysis was done using Image-Pro Plus V.4.1. (Media Cybernetics, L.P, MD, USA). To determine volume fraction and surface area of the aluminide alumina phases, a quantitative characterization of the microstructure using Image Analysis software was performed. Soon after image acquisition, the image has been converted to binary image to perform the measurements. Segmented the binary image by thresholding the histogram in to various phases of interest. Then performed the measurements using area and perimeter of the threshold images for obtaining volume fraction and surface area of phase of interests. Area per area ($\overline{A_A}$) gives volume per volume (V_v), volume fraction of the phase. Perimeter gives the L_A that can be related to S_v using ($4/\pi$. L_A).

CHAPTER 4:RESULTS AND DISCUSSION

4.1 Introduction

Alumina Aluminide Alloys (3A) composites experiment started with different compositions of aluminum and Titania molar ratios. Experiments started with a view to produce Ti_xAl_y intermetallic and Al_2O_3 composites in situ by mechanical milling, hot pressing and heat treatments. Characterization of these composites involved XRD, EPMA, Optical microscopy, four point bent testing, microhardness and Image analysis (quantitative microscopy). These characterization results are discussed in the following sections.

4.2 X-Ray diffraction and DSC

X-Ray diffraction patterns of the processed (mechanical milled, hot pressed and heat treated) samples of composition C3 (1: 0.18 mol%) and C4 (1:0.17 mol%) are shown in ***Fig. 4.1 and Fig. 4.2.*** Composition of samples under study and their identification numbers are shown in ***Table 4.1*** (same table as Table 3.1). Phase evolution of alumina aluminide alloy composite demonstrate that the initial powders reacts at temperature below 660 °C (melting point of Al) and forming different types of aluminides under the influence of thermodynamics and kinetics. The evidence of solid state reaction in the process realized by DSC (differential scanning Calorimetry) experiment in which the reaction starts below melting point of aluminum. Observe the DSC data of C4 sample shown in ***Fig. 4.3.***

Phase evolution of composition C3 shown in ***Fig. 4.1*** resulted with $TiAl_3$ and Al_2O_3 from JCPDS standard peak values after mechanical milling (*MM*) and different heat treatment times as labeled in the figure.

XRD analysis after mechanical milling, aluminum and TiO_2 were seen, though peaks for TiO_2 broadened and less prominent. This is due to amorphisation of TiO_2 during mechanical milling. No peaks for intermetallics were seen indicating no chemical reaction and or mechanical alloying (though small fractions of phases can be missed in XRD).

In hot pressing things that are seen are aluminum, α-Al_2O_3 and $TiAl_3$. It looks TiO_2 presence can not be conformed on the hot pressed sample. At 2θ= 38.7 $TiAl_3$ peaks are seen. Intensity of $TiAl_3$ peak decreased in the 27-hour sample. Ti_3Al and Ti_2O_3 were not present. The intensity of peaks of Al_2O_3 increased through out. The peaks at 2θ= 33.4, 44.8, 51.0, 54.5 and 61.4 could not be identified with the available JCPDS standard charts.

Where as in case of C4 (***Fig. 4.2***) the phases formed are Ti_9Al_{23} and Al_2O_3. However, small peaks of aluminum are observed in C4 sample indicating unreacted aluminum. This is likely since C4 contains the maximum amount of aluminum among the samples. Though aluminum could not be identified under optical microscopic survey. XRD analysis after mechanical milling, aluminum and TiO_2 were seen, though peaks for TiO_2 broadened and less prominent. This is due to amorphisation of TiO_2 during mechanical milling. No peaks for intermetallics were seen indicating no chemical reaction and or mechanical alloying. In hot pressing things that are seen are aluminum, α-Al_2O_3 and $TiAl_3$. It looks TiO_2 presence can not be conformed on the hot pressed sample. At 2θ= 38.7 $TiAl_3$ peaks are seen. Ti_3Al and Ti_2O_3 was not present. The intensity of peaks of Al_2O_3 increased through out.

Moreover, some unidentified peaks were present which needs further study. After sufficient time of heat treatment, equilibrium aluminide phases were formed (In case of C3 $TiAl_3$ and Al_2O_3 and in case of C4 Ti_9Al_{23} and Al_2O_3). The XRD peaks are seen to evolve with time of heat treatment indicating that the reaction is not complete at lower times. This is expected because of slow kinetics in solid state reactions. Compositions

studied in the present work and corresponding phases identified (XRD study) experimentally are tabulated. Also theoretically predicted phases (based on reaction sequence [66] proposed in the literature) are presented in ***Table 4.2 and Table 4.3***

4.3 Optical Microscopy and EPMA

Microstructures of composition C3 and C4 are shown in ***Fig. 4.4***, ***Fig. 4.5*** and ***Fig. 4.6*** after reaction sintering at 1400°C in vacuum for different durations at different magnifications. The phases present in the microstructure are black (Al_2O_3), grey and white (both aluminides). Fine distribution of interconnected aluminide alumina is seen. Micrographs show uniform distribution of alumina and aluminides. Amount of porosity present in the microstructure varied from 15-20 vol%(using quantitative microscopy). Applying pressure during cooling cycle of the hot pressing operation could minimize the amount of porosity in the microstructure (~ apply pressure at about 600°C). During heating cycle if one tries to apply more pressure, liquid aluminum oozes out along the graphite die wall and punch interfaces. Amount of aluminum loss during hot pressing has been taken care of while calculating the molar ratios of Al and TiO_2 compositions. Co-continuous network of structure is clearly seen in the microstructure. EPMA (Electron Probe Micro Analyzer) dot mapping clearly shows the distribution of aluminum and titanium in the microstructure, is one of the evidence of formation of aluminides. Dot maps of different compositions for different durations are shown in figures (***Figs. 4.7, 4.8, 4.9, 4.10*** and ***4.11***). Qualitative point analyses on separate phases indicate the presence of aluminide formation in the microstructure (***Fig. 4.12)*** and alumina formation ***(Fig. 4.13).*** Line analysis has been performed on the specific microstructure (***Fig. 4.14***) for conforming the variation of composition along the line (diffusion of the species in one another). Qualitative Analysis is presented to relatively estimate the individual concentrations of the aluminum and titanium on individual phases.

4.4 Bulk Density

Bulk density of the sintered samples was determined using Archimedes principle in water. Composition of the sample used, initial weight and weight loss in water and density are presented in ***Table 4.4***. We compared the theoretical densities of the samples based on mass balance (***Table 4.5***). Theoretical density values were higher in all the cases which is a expected since porosity is present in the samples. The following assumptions were made when calculating theoretical densities,

(i) No unreacted TiO_2 was present in any of the samples.

(ii) In C1 composition no $TiAl_3$ was present, only Al_2O_3, TiAl and Ti_3Al were present.

(iii) In C3 and C4 only Al_2O_3, aluminum, and $TiAl_3$ were present.

(iv) In case of C2, there was no aluminum present and only Al_2O_3, $TiAl_3$ and TiAl were present.

(v) Lastly, for CT3, no Ti_3Al and only Al_2O_3, $TiAl_3$ and TiAl were present.

These are derived from the reaction sequence proposed by [66] assuming that all the reactions go to completion.

Modulus values were measured using ultrasonic tester. The values are presented in *Table. 4.6.* Extremely low values of modulus are seen which is attributed to reflections due to high porosity in the composite (without porosity this method holds good).

4.5 Microhardness Testing

Microhardness was measured using Vickers diamond pyramid (knoop) testing. There is a wide variation of hardness values with varied composition and also on individual phases. Vickers hardness values using 60g weight results were varying from 5GPa to 22GPa. Some of the values are comparable with literature [14,63,69] and others are lower. Probable reasons could be more aluminum content present and porosity. Measures densities are shown in ***Table. 4.7.***

4.6 Four Point Bend Testing

Fracture toughness values obtained are ~4.0 Mpa$\sqrt{m}$. Flexural strength values vary from 80 to 345 Mpa. Composition of the sample used for testing was Al: TiO_2 = 1: 0.187 and 1: 0.5695 (PC4 and PC1 in ***Table 4.1*** respectively). These strength values can be improved by decreasing the porosity through process control and proper selection of the initial powder composition. Similar tests could not be performed at other compositions because the rectangular samples required for testing suffered from distortion and lamination defects. After hot pressing, there would be uneven distribution of porosity in the sample, due to aluminum loss. It is thought that this distribution of porosity led to uneven shrinkage during sintering (heat treatment process) resulting in sample distortion. It is felt that variation of density distribution during the process of hot pressing has attributed to lamination defects.

4.7 Scanning Electron Microscope

SEM (Scanning Electron Microscope) micrograph shows the nature of crack propagation of notched and unnotched four point bend test samples (***Fig.4.15*** and ***Fig. 4.16***). It can be observed from ***Fig. 4. 15. (d)*** that the samples failed along the grain boundaries. Crack deflection (typical composite behavior) can be clearly seen on fractured samples shown. Micrograph shown in ***Fig 4.17*** shows the indentation made on the grey phase. Crack formed on the grey phase when indentation was made with 100g load for 5 seconds using Vickers diamond pyramid testing. It conforms that the grey phase is brittle.

4.8 Measurement of V_V and S_V using digital image analysis

To determine volume fraction (V_V) and surface area (S_V) of the aluminide and alumina phase, a quantitative characterization of the microstructure using Image Analysis software was performed. Digital Image analysis was done using Image-Pro Plus V.4.1. Win 95/98 &NT 4.0 (Media Cybernetics, L.P, MD, USA). After image acquisition, image enhancement operations were performed. Grey scale image was segmented to a binary image by thresholding the image at various grey scales. These grey scales were selected based on the frequency histogram of the grey scale levels in the image. This resulted in segmented binary images of various phases (in this case three). Thresholding was done on the histogram as indicated in the ***Fig. 4.18.*** Volume fraction was measured by area fraction method which states that mean area fraction of a phase (Area per area) is equal to volume fraction (volume per volume V_V) of the phase. Perimeter of the phase of interest can be related to a quantity L_A which provides an estimate of surface area per unit volume ($S_V = 4/\pi . L_A$). Histogram of the microstructure (grey scale values distribution), the initial microstructure and images after thresholding are shown in ***Fig.4.18*** and ***Fig. 4.19.*** The results of this measurement are provided in ***Table.4.8.***

CHAPTER 5:CONCLUSIONS

The following conclusions were made from the present research work

1. Different aluminides (Ti_xAl_y) can be made possible by adjusting the starting composition of the powders (Al and TiO_2).
2. Differential Scanning Calorimetry conforms that the solid state reaction operates in 3A process much below melting point of aluminum.
3. TiO_2 is not present at all, in any of the samples, which shows high affinity of aluminum for oxygen.
4. We were conclusively able to form TiAl using Alumina Aluminide Alloy Process (3A).
5. Other intermetallics that were formed are$TiAl_3$ and Ti_9Al_{23} though Ti_3Al could not be resolved because of overlapping of peaks.
6. The theoretical density calculated by mass balance is always more than measured density.
7. Porosity in these samples was of the order of (15-20%).
8. Measured fracture toughness was of the order of 4.0 MPa$\sqrt{m}$ and flexural strength shows wide variation from 80 to 345 MPa.

GUIDELINES FOR FUTURE WORK

1. Addition of micro alloying elements (Refractory metals) such as V, Nb, Cr on the 3A process can be studied.
2. Slurry casting of the powders followed hot rolling can be introduced to control the porosity in these composites.
3. A systematic study of the dependence of kinetics of the 3A process on powder size (coarse to nanosize powders) should be undertaken.
4. External addition of diluents like ZrO_2 and Al_2O_3 can be studied to tailor the volume fraction of the ceramic phases.

Table.1.1 Classification of in situ composites.

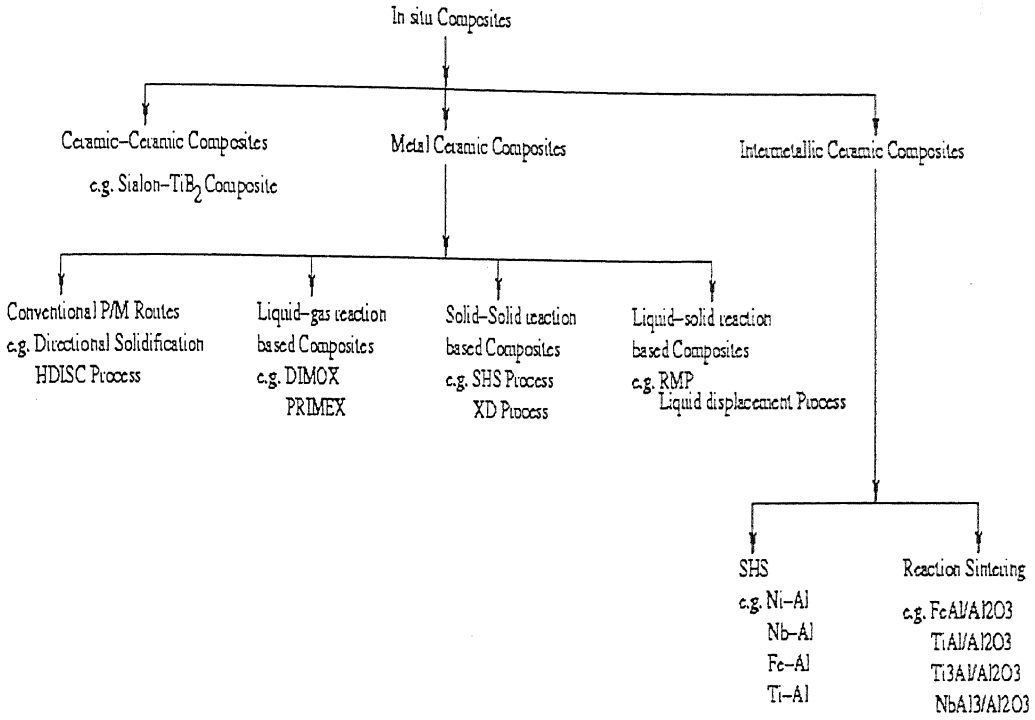

Table. 2.1. Adiabatic Temperatures for the Combustion Synthesis of Selected Compounds [11].

Compound	T_{ad} (K)	Compound	T_{ad} (K)
TiB_2	3190	TiN	4900
ZrB_2	3310	ZrN	4900
NbB_2	2400	HfN	5100
TaB_2	3370	NbN	3500
MoB	1800	TaN	3360
LaB_6	2800	Si_3N_4	4300
B_4C	1000	BN	3700
Al_4C_3	1200	AlN	2900
TiC	3210	Be_3N_4	3200
HfC	3900	Ti_5Si_3	2500
TaC	2700	Zr_5Si_3	2800
SiC	1800	$NbSi_2$	1900
WC	1000	$MoSi_2$	1900

Table 2.2. Enthalpies of 3A Synthesis Reactions [15,72,74,75].

Synthesis Reaction	ΔG (Kg/mol)	ΔH (Kg/mol)
$1.5TiO_2+2Al \rightarrow 1.5Ti+Al_2O_3$	-248.164	-258.6
$Ti+3Al \rightarrow TiAl_3$	-139.4	-146.4
$3Nb_2O_5+2Al \rightarrow 2Nb_2O_5+Al_2O_3$	-719.5	-746.8
$0.6Nb_2O_5+2Al \rightarrow 1.2Nb+Al_2O_3$	-547.3	-536.0
$1.5NbO_2+2Al \rightarrow 1.5Nb+Al_2O_3$	-473.5	-483.3
$Nb+3Al \rightarrow NbAl_3$	no data	-132.0
$Fe_2O_3+2Al \rightarrow 2Fe+Al_2O_3$	-840.0	-851.4
$Fe+Al \rightarrow FeAl$	no data	-50.2
$Mo+2Si \rightarrow MoSi_2$	--	-131.8

Table 2.3. Phase change thermodynamic properties of oxides [76].

Oxide	Phase	Transition temperature (K)	Heat of transition (Kcal.g /mol)	Entropy of transition(e.u)
TiO	Solid, α Solid, β	1264 dec.2010	0.82 --	0.65 --
Ti_2O_3	Solid, α Solid, β Liquid	473 2400 3300	0.215 (24)	0.455 (10)
Ti_3O_5	Solid, α Solid, β Liquid	450 (2450) (3600)	2.24 (50) (85)	4.98 (20) (24)
TiO_2	Solid Liquid	2128 dec.3200	(16)	(7.5)
Ti_2O	Solid Liquid	573 773	(5.0) (17)	(8.7) (22)

पुरुषोत्तम कालीनाथ केलकर पुस्तकालय
भारतीय प्रौद्योगिकी संस्थान कानपुर
अवाप्ति क्र० A 137951

Table 2.4. Properties of different 3A Systems [14,63-66].

S.No	Composition	Bending Strength, MPa	VHN, GPa	Overall Shrinkage
1	45vol% TiO_2-55vol%Al	420±32	16.5	13
2	66.4Al-33.6vol% Nb_2O_5	445	14.6± 0.2	11
3	29.2Al-54.8 Al_2O_3	-	-	5
4	16.8Al-65.1 Al_2O_3-18.1Fe	570	5.7	15
5	7.4Al-22.6Fe-70 Al_2O_3	700	-	-
6	20ZrO2-35 Al_2O_3-45Al	410	-	8

Table 2.5. Amorphous phases formed in blended powder mixtures of Ti-Al by MA [82-84].

System	Vial Material	Grinding (medium m/l)	BPR	MA time(h)
Ti-25Al	Hardened Steel	-	-	9-16
Ti-25Al	WC	-	8:1	20-24
Ti-25Al	S.S	S.S	100:1	50
Ti-25Al	S.S	S.S	5:1	25
Ti-50Al	S.S	Hardened Steel	70:1to 100:1	75
Ti-50Al	S.S	S.S	18:1	20
Ti-50Al	S.S	440 C Steel	40:1	500
Ti-50Al	S.S	S.S	30:1to 60:1	80
Ti-60Al	Hardened steel	Hardened steel	10:1	25-30
Ti-Al	Hardened steel	Hardened steel	10:1	40
Ti-48Al-2Cr	-	S.S	30:1	500
Ti-40Al-10Ni	Steel	Steel	8:1	40
Ti-25Al-25Ni	Steel	Steel	8:1	20
Ti-20Al-20Ni	Steel	Steel	8:1	40
Ti-15Al-15Ni	Steel	Steel	8:1	20

Table 2.6. Properties of titanium aluminides, titanium base conventional alloys and superalloys [92,93].

Property	Ti_3Al	TiAl	Ti base	Superalloys
Density (gm/cm^3)	4.1-4.7	3.7-3.9	4.5	8.3
Modulus (GPa)	100-145	160-176	96-100	206
Yield strength (MPa)	700-990	400-650	380-1150	-
Tensile Strength (MPa)	800-1140	450-800	480-1200	-
Creep limit (°C)	760	1000	600	1090
Oxidation limit (°C)	650	900	600	1090
Ductility at RT (%)	2-10	1-4	20	3-5
Ductility at HT (%)	10-20	10-60	High	10-20

Table 2.7. Room Temperature and elevated temperature Properties of Ti_3Al [95].

Alloy	Y.S (MPa)	UTS (MPa)	%E	K_{IC} MPa$\sqrt{m}$	Creep Strength
Ti-25Al	538	538	0.3	--	-
Ti-24Al-11Nb	787	824	0.7	--	44.7
	761	967	4.8	--	--
Ti-24Al-14Nb	831	977	2.1	--	59.5
Ti-24Al-14Nb-3V-0.5Mo	--	--	26	--	--
Ti-25Al-10Nb-3V-Mo	825	1042	2.2	13.5	360
Ti-24.5Al-17Nb	952	1010	5.8	28.3	62
	705	940	10.0	--	--
Ti-25Al-17Nb-Mo	989	1133	3.4	20.9	476
Ti-15Al-22.5Nb	860	963	6.7	42.3	0.9
Ti-23.5Al-24Nb	960	--	--	--	--

Table 2.8. Properties of γ-based TiAl by various techniques [128,134,139-142].

Material/ Composition/ Alloy	Processing	Properties Temp (°C)	$\sigma_{0.2}$ (MPa)	UTS/σ_F	E (%)	Micro structure
Ti-48Al-2Nb-2Cr	Laser Formed	R.T	550	585	1.5	FL
Ti-48Al-2Nb-2Cr	PM + HT	R.T	510	597	2.9	NL
Ti-48Al-2Nb-2Cr	PM + HT	760	----	----	----	NL
Ti-48Al-2Nb-2Cr	PM+HIP+HT	R.T	340	380	0.5	FL
Ti-48Al-2Nb-2Cr	PM+HIP+HT	760	----	----	----	FL
Ti-48.9Al	Spray formed	R.T	378±20	466±20	1.3±0.2	NL ~100μm
TI-48Al	Cast	R.T	350	370	1.0	FL, >400μm
TI-48Al	Extrusion +HT	R.T	360	441	1.7	NL 300μm
Ti-45Al-10Nb	Extruded 1300 °C	R.T 700 °C	1052 679	1069 >834	0.78 >5.4	---- ----
Ti-47Al-2Nb-Cr-0.2B	Forging+ HT	R.T R.T	426 384	541 489	0.8 0.94	FL Duplex

FL=Fully Lamellar NL=Nearly Lamellar HT=Heat Treatment HIP= Hot Isostatic Pressing PM=Powder Metallurgy

Table 3.1 Selected compositions of the powders.

Sample designation	Composition (Al:TiO_2:Ti moles)
C1	1: 0.56: 0
C2	1: 0.31: 0
C3	1: 0.18: 0
CT3	1: 0.18: 0.11
C4	1: 0.17: 0
PC1	1: 0.569: 0
PC2	1: 0.390: 0
PC3	1: 0.291: 0
PCT3	1: 0.199: 0.128
PC4	1: 0.187: 0

Table 3.2 XRD settings used for characterization of powders and 3A composites.

Parameter	Setting
Voltage	30kV
Current	20mA
Scanning Speed (2θ)	3°/min
Time constant	10sec
Counts/min	5 K

Table 4.1 Compositions and sample identification used in this study.

Sample designation	**Composition** (Al:TiO_2:Ti moles)
C1	1: 0.56: 0
C2	1: 0.31: 0
C3	1: 0.18: 0
CT3	1: 0.18: 0.11
C4	1: 0.17: 0
PC1	1: 0.569: 0
PC2	1: 0.390: 0
PC3	1: 0.291: 0
PCT3	1: 0.199: 0.128
PC4	1: 0.187: 0

Table 4.2. Theoretical reaction sequence of initial powder composition.

Al:TiO_2 (mol%)	**Possible Reaction Sequence**
1 : 0.230	1.0 Al+ 0.230 TiO_2 → 0.230 $TiAl_3$ + 0.154Al_2O_3
1 : 0.410	0.197TiO_2 +0.230 $TiAl_3$ → 0.427 TiAl + 0.1314Al_2O_3
1 : 0.582	0.171 TiO_2 + 0.437 TiAl → 0.199 Ti_3Al +0.113Al_2O_3
1 : 2.982	2.388 TiO_2 + 0.199 Ti_3Al →1.492 Ti_2O_3 + 0.099Al_2O_3

Table 4.3. Theoretically expected / Experimentally Observed Phases using XRD.

Al:TiO_2 (moles)	Al_2O_3		$TiAl_3$		TiAl		Ti_3Al		Ti_2O_3	
	The.	Exp	The.	Exp	The.	Exp	The.	Exp	The.	Exp
1: 0.56	Y	Y	N	Y	Y	? /Y	Y	? /Y	N	N
1: 0.31	Y	Y	Y	Y	Y	?	N	N	N	N
1: 0.18	Y	Y	Y	Y	N	N	N	N	N	N
1: 0.17	Y	Y	Y	Y/Ti_9Al_{23}	N	N	N	N	N	N
1: 0.18	Y	Y	Y	Y/Ti_9Al_{23}	Y	Y/?	N	N	N	N
1: 0.569	Y	Y	N	Ti_9Al_{23}	Y	N	Y	N	N	N
1: 0.390	Y	Y	Y	N	Y	Y	N	N	N	N
1: 0.291	Y	Y	Y	Y	Y	Y/?	N	Y/?	N	N
1: 0.199	Y	Y	Y	Ti_9Al_{23}	N	Y/ Ti_9Al_{23}	N	N	N	N
1: 0.187	Y	Y	Y	N	N	N	N	Y/?	N	N

Table 4.4 Measured densities of 3A Samples.

S.N0	Al: TiO_2 (mole)	S.ID	Initial Wt	Wt loss in water	Density (gm/cc)
1	1: 0.556	PC1	0.8681	0.2543	3.4136
2	1: 0.181	CT3	1.1624	0.3759	3.0923
3	1: 0.183	C3	1.2486	0.3608	3.4606
4	1: 0.174	C4	1.1963	0.3986	3.00125
5	1: 0.174	C4	0.9687	0.2842	3.4085

Table 4.5 Theoretical densities versus measured densities.

Sample Identification	Measured Density	Theoretical Density
C1	3.41	4.10
C3	3.46	3.27
CT3	3.09	3.39
C4	3.00	3.25

Table 4.6 Modulus values of the samples using ultrasonic testing.

Al: TiO_2 (Molar Ratio)	S.ID	Initial Wt	Wt loss in water	Time(nanoseconds)	Density	Modulus (GPa)
1: 0.556	PC1	0.8681	0.2543	1270	3.4136	60
1: 0.181	CT3	1.1624	0.3759	780	3.0923	48
1: 0.183	C3	1.2486	0.3608	620	3.4606	49.2
1: 0.174	C4	1.1963	0.3986	780	3.00125	59.7

Table 4.7 Micro hardness of individual phases (Kg/mm^2).

Sample ID	White	Grey	Black	Al: TiO2: Ti
C4	700.6803	810.1222	810.1222	1: 0.17: 0
C3	650.9669	729.5603	434.4136	1: 0.18: 0
C2	1017.086	925.7212	402.1321	1: 0.31: 0
C2	511.8418	385.9127	427.6581	1: 0.30: 0
PC2	257.3066	589.7424	729.5603	1: 0.39: 0
PC3	2119.252	1842.545	384.4482	1: 0.29145: 0
PCT3	818.909	1245.654	1129.834	1: 0.199: 0.128
PC4	1245.654	1245.654	642.6052	1: 0.187: 0

Table 4.8 Measured V_V (volume fraction) and S_V of samples at 200X magnification.

S.ID	Gray Vv	White Vv	Grey Sv	White Sv
C2	67.2	11.4	0.000419	0.000606
CT3	41.5	33	0.000435	0.000491
C3	45.2	8	0.000214	0.00067
C4	46.6	17.3	0.001675	0.000395
C4	32.2	17	0.000214	0.000675

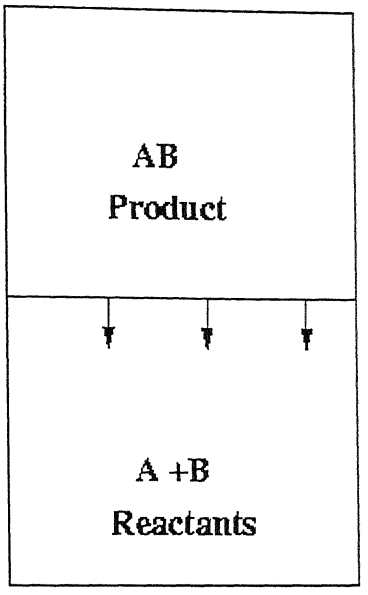

Fig. 2.1(a) Schematic representation of SHS process.

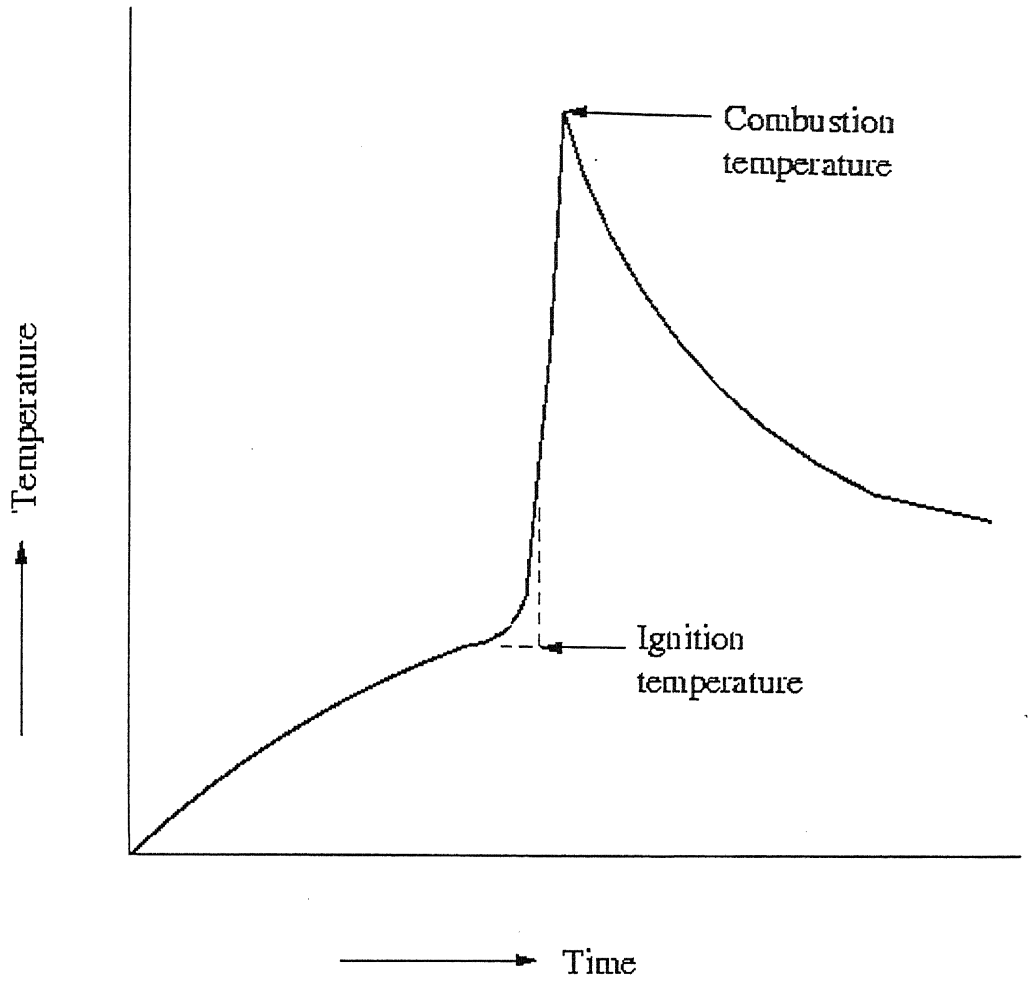

Fig. 2.1(b) Schematic representation of the temperature profile associated with passage of a combustion front [11].

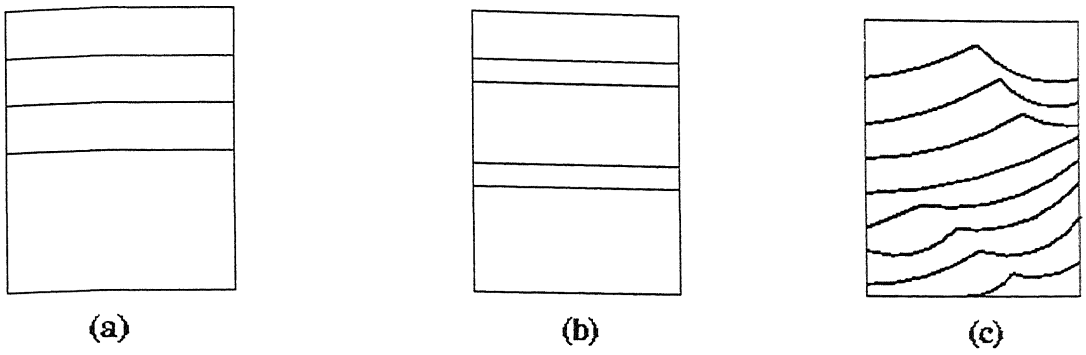

Fig. 2.1(c) Schematic representation of combustion wave propagation: (a) steady state (b) oscillatory (c) spin.

Route (a)

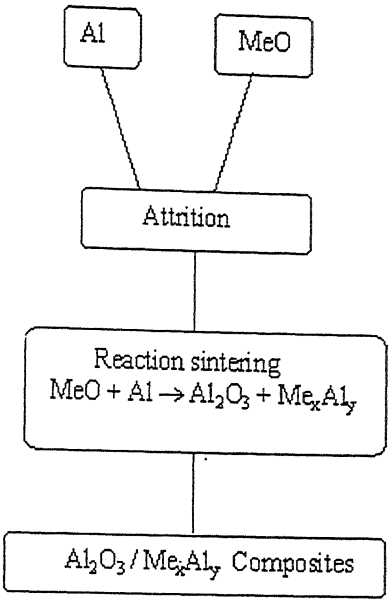

Route (b)

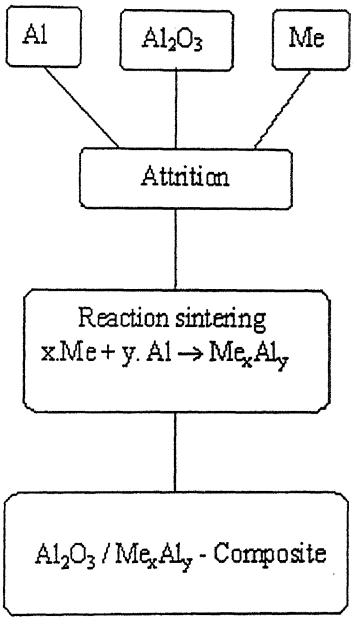

Fig. 2.2 Two different 3A processing routes.

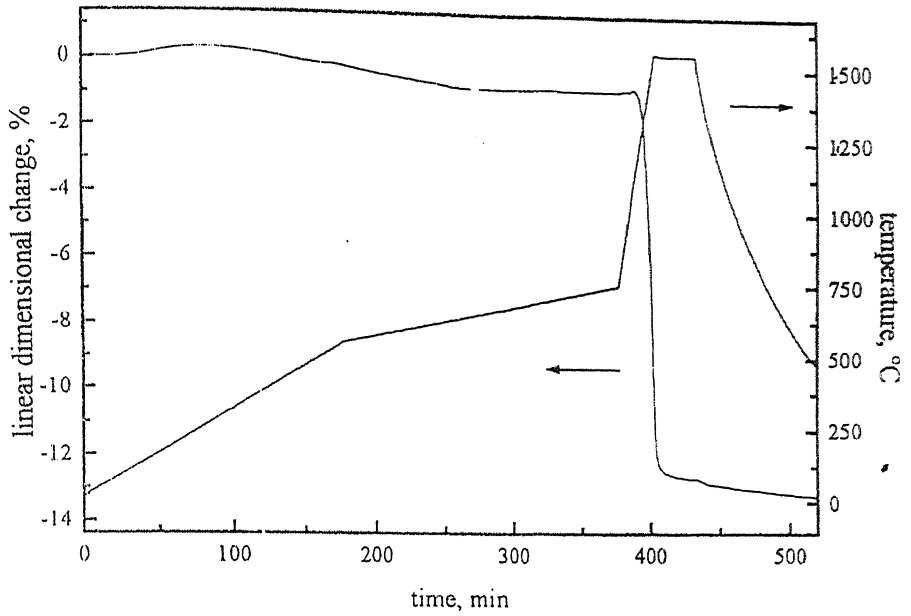

Fig. 2.3 Linear dimensional change of 55 vol% Al and 45 vol% TiO_2 heated in vacuum to a maximum temperature of 1550 °C [43].

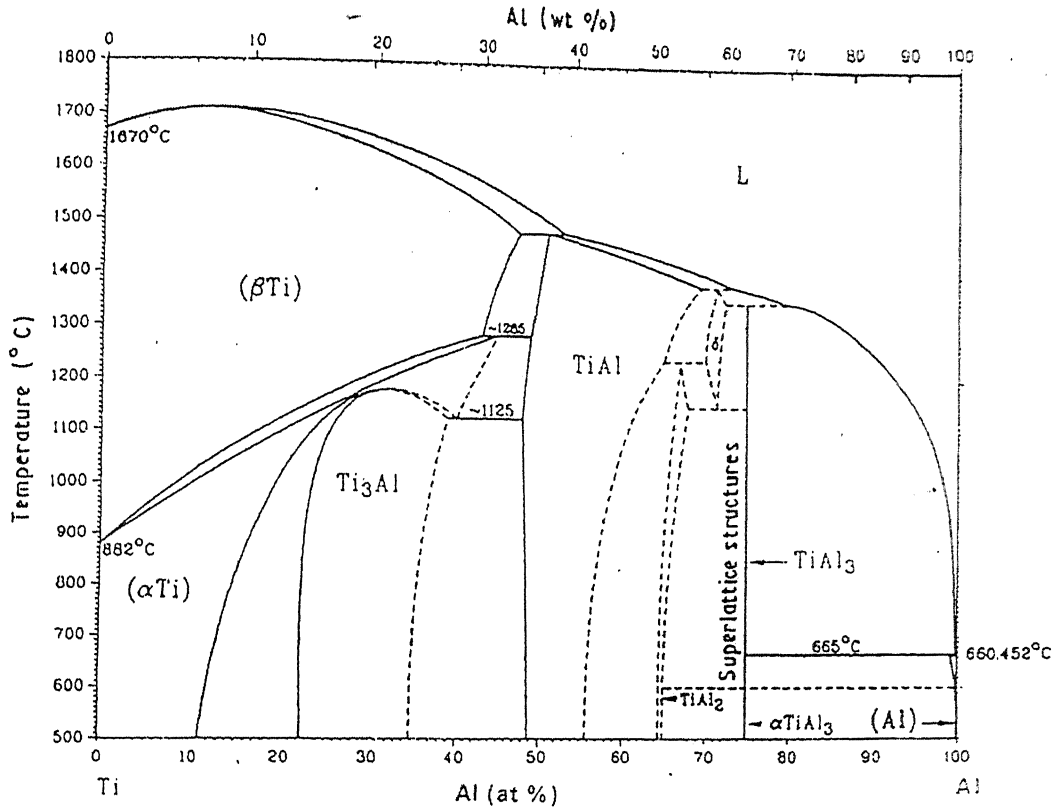

Fig. 2.4 Schematic representation of Ti-Al phase diagram [86].

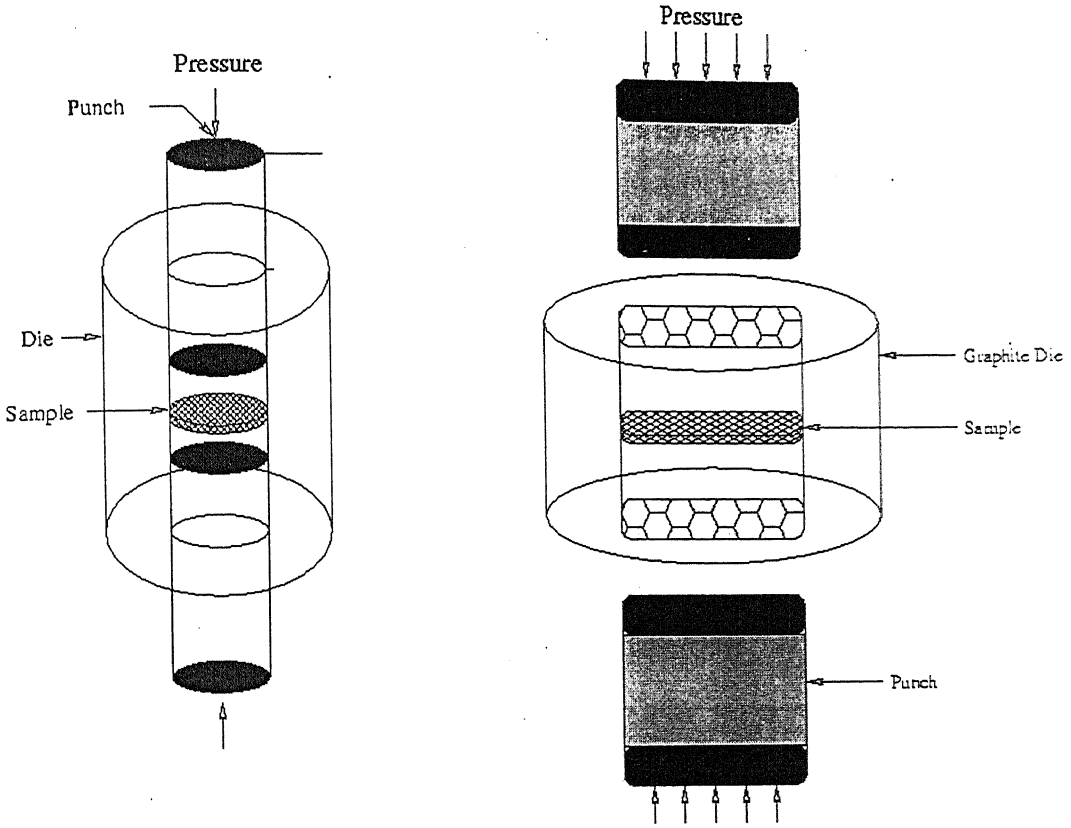

Fig. 3.1 Schematic of graphite dies and punches used for hot pressing.

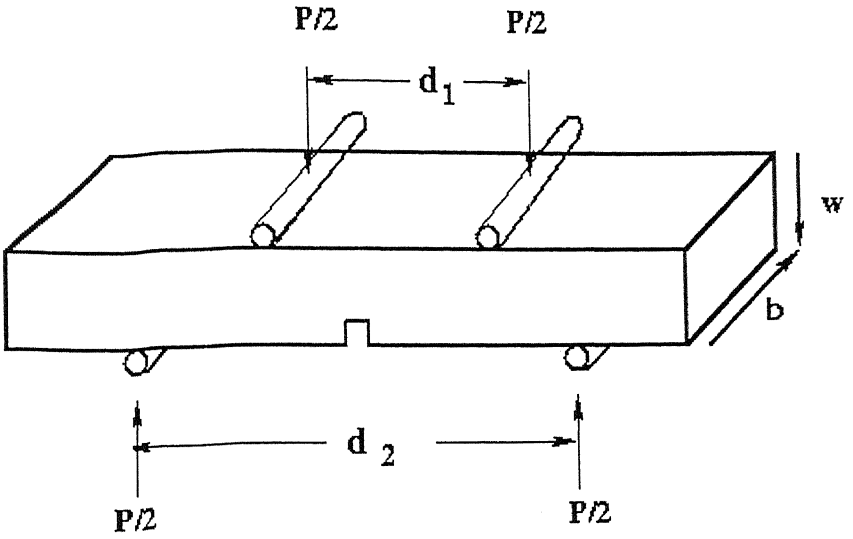

Fig. 3.2 Schematic of four point bending arrangement to measure strength and toughness of beam specimen.

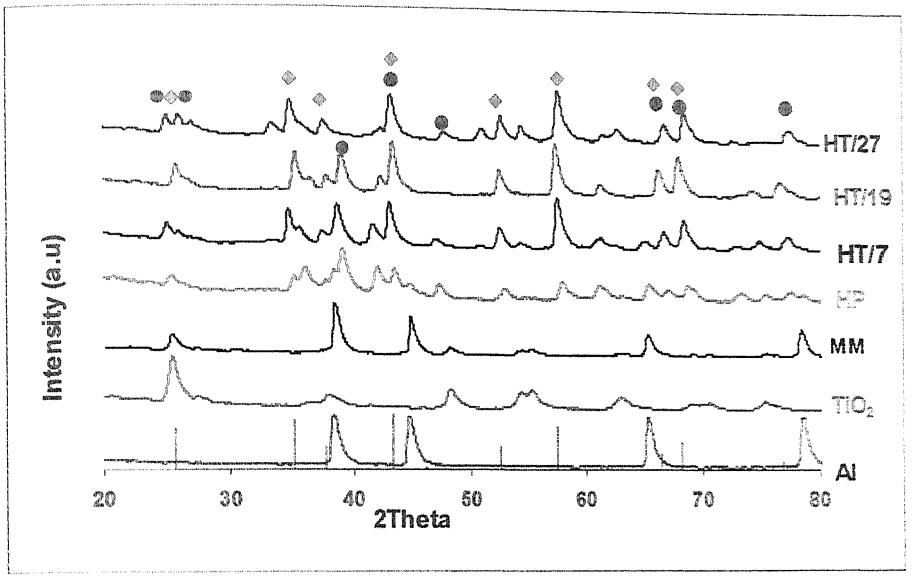

Fig. 4.1. Phase evolution of C3 (Al: TiO_2=1: 0.18) after mechanical milling, Hot pressing and different heat treatments. Vertical lines correspond to standard Al_2O_3 peaks. Red colour diamond indicates Al_2O_3 and green indicates $TiAl_3$ peaks.

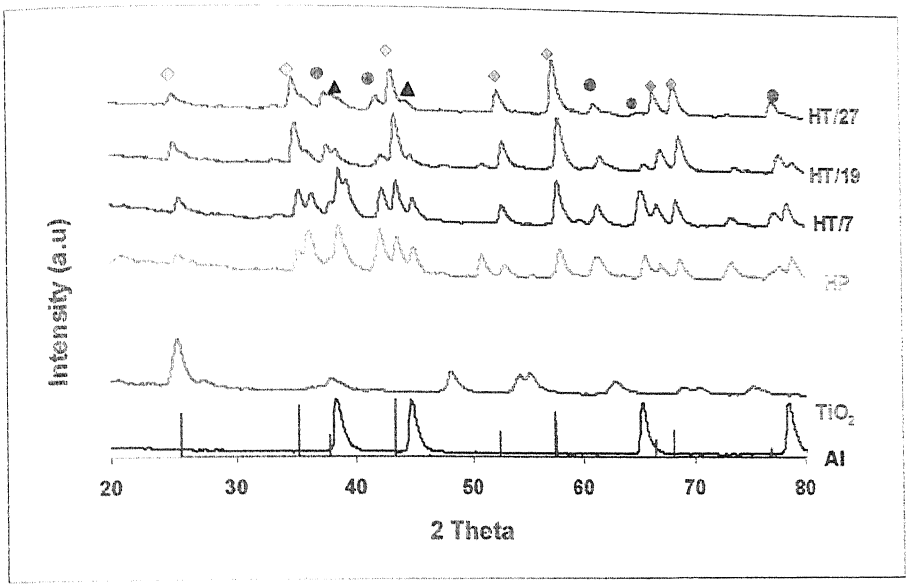

Fig. 4.2. Phase evolution of C4 (Al: TiO_2=1: 0.17 mole) after mechanical milling, hot pressing and different heat treatments. Vertical lines correspond to standard Al_2O_3 peaks. Red colour diamond indicates Al_2O_3, green indicates Ti_9Al_{23} and black triangle is residual aluminium peaks.

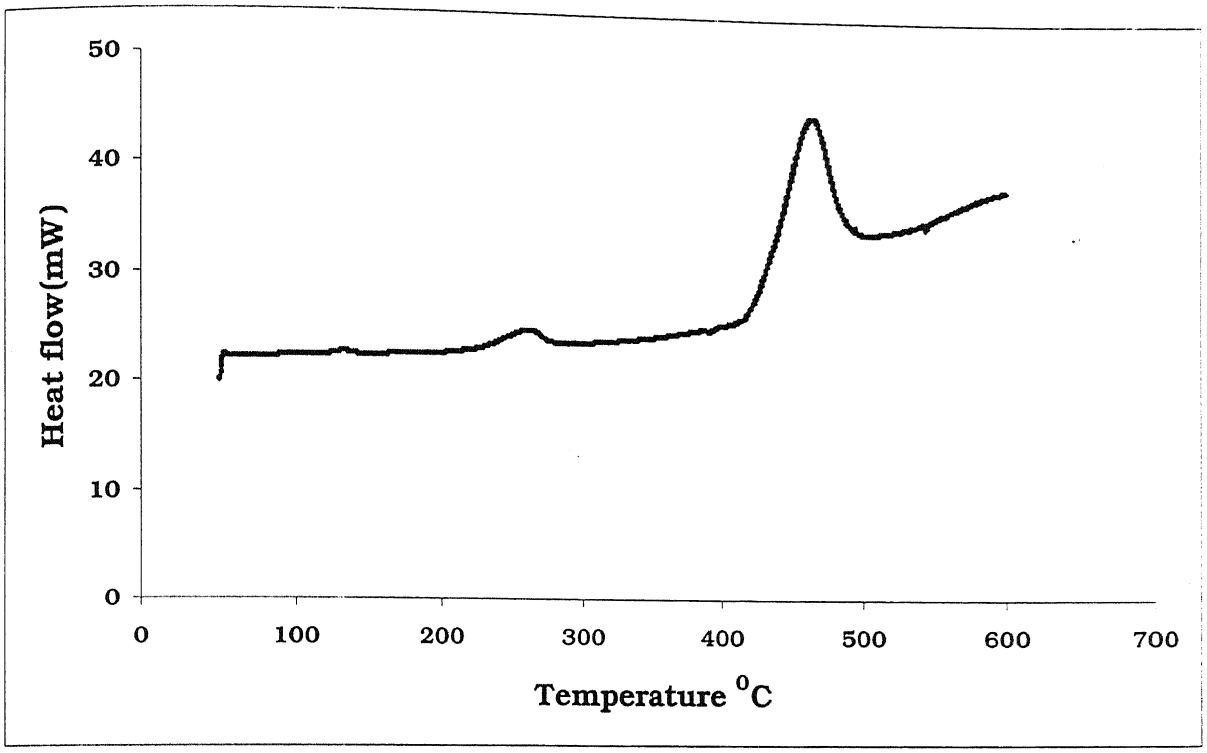

Fig. 4.3 DSC data for C4 composition. An exothermic reaction is observed between 450 and 500 °C.

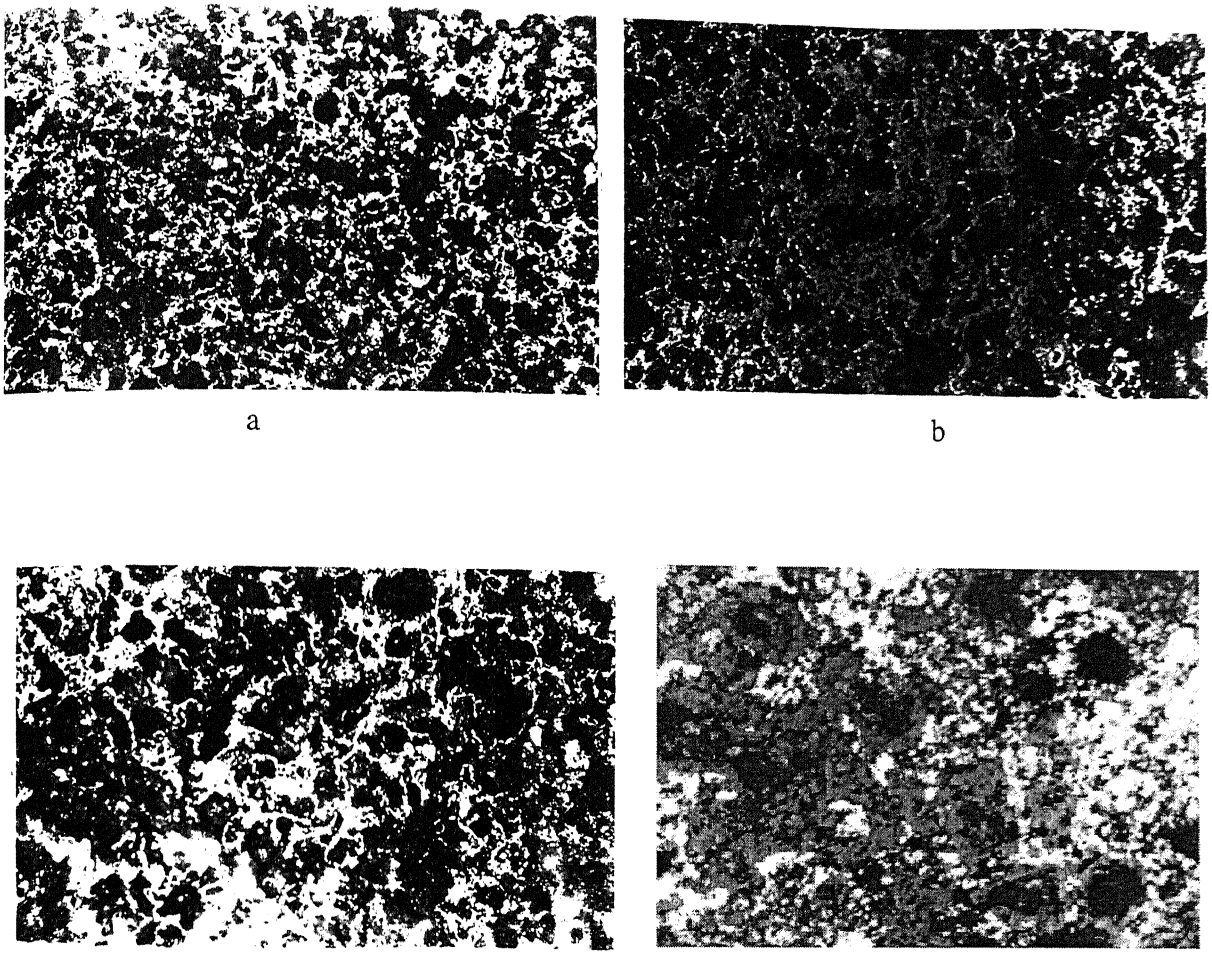

Fig.4.4 Shows the optical micrograph of C3 sample (Al: TiO_2=1: 0.18 mole) heat treated at 1400 °C in vacuum for different duration's. (a) Micrograph of specimen heat treated for 7 hours at 50X (b) heat treated for 7 hours at 100X (c) heat treated for 7 hours at 200X. Fine distribution of interconnected aluminide alumina is seen. (d) heat treated for 24 hours at 100X.

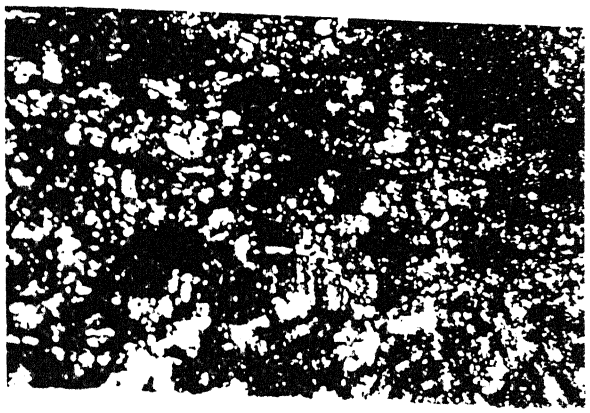

a

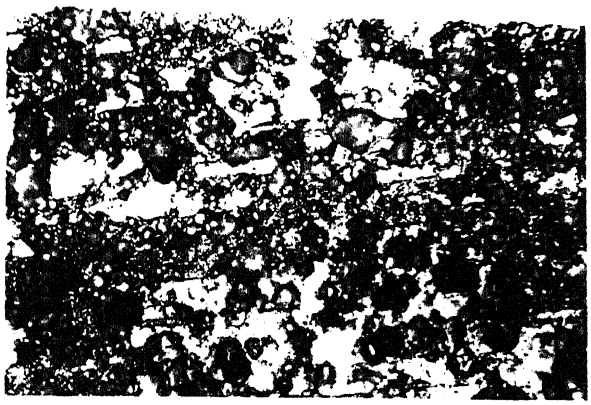

b

Fig. 4.5 Shows the optical micrograph of C4 sample (Al: TiO_2=1: 0.17 mole) heat treated for 7 hours at 1400 °C in vacuum. (a) at 200X (b) at 500X. Micrograph shows the fine uniform distribution of alumina and aluminides. Also they are mutually interconnected.

a

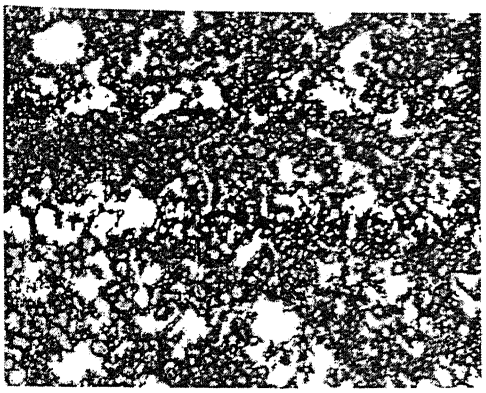

b

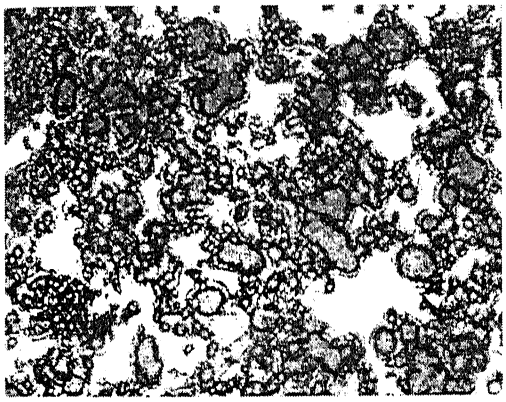

c

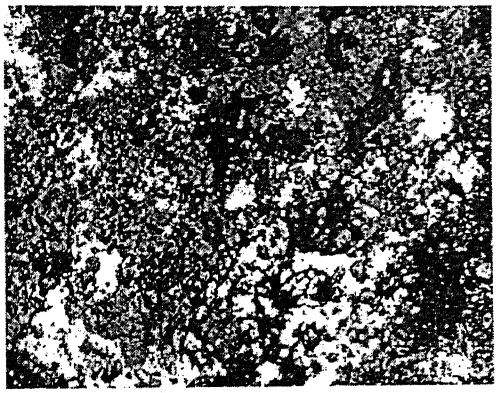

d

Fig.4.6 Shows the optical micrograph of C4 sample (Al: TiO_2=1: 0.17 mole) heat treated at 1400 °C in vacuum for different duration's. (a) micrograph of specimen heat treated for 7 hours at 100X (b) heat treated for 19 hours at 100X (c) heat treated for 19 hours at 200X (d) heat treated for 24 hours at 100X.

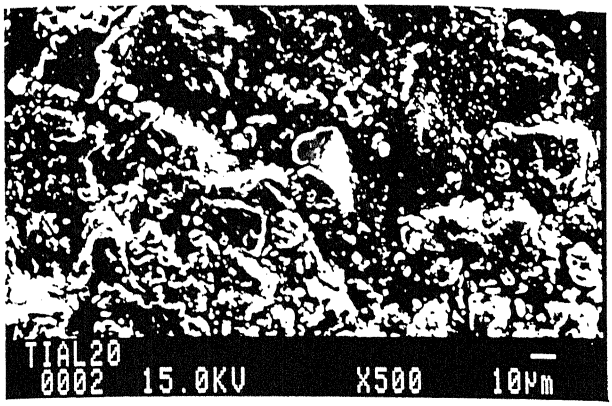

a

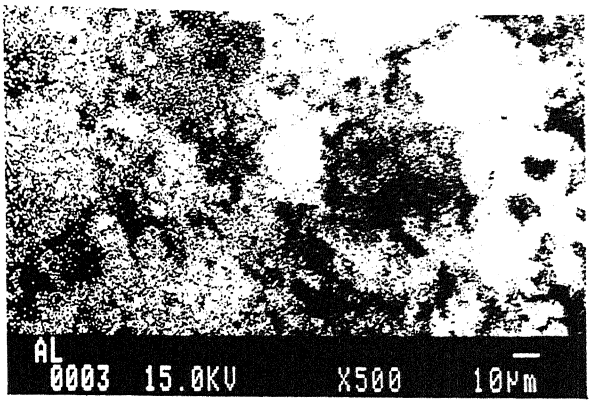

b

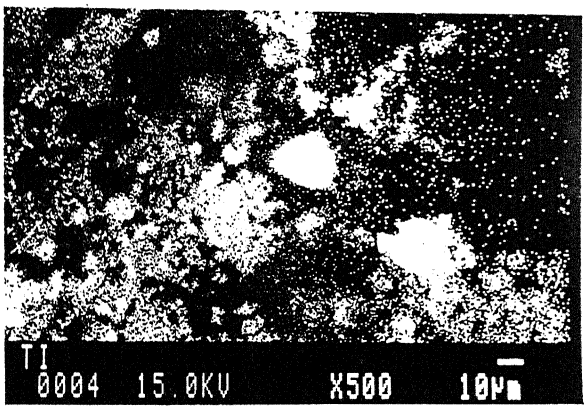

c

Fig.4.7 EPMA dot mapping of C3 sample (Al: TiO_2=1: 0.18 mole) heat treated for 7 hours at 1400 °C in vacuum. (a) Microstructure on which dot mapping was performed. (b) Dot map of aluminium (c) dot mapping of titanium. Dot mapping indicates that the dark phase is Al_2O_3 and grey phase is aluminides (These have been independently checked by point analysis also).

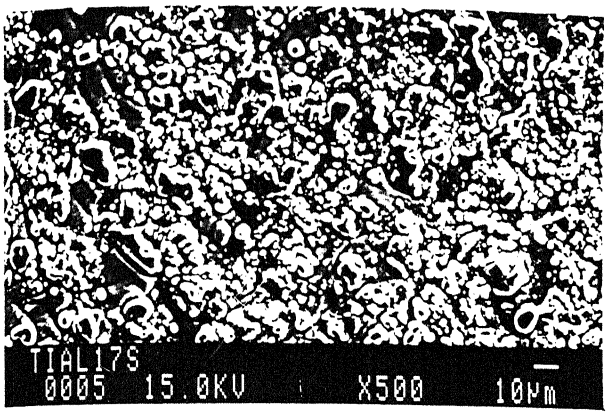

a

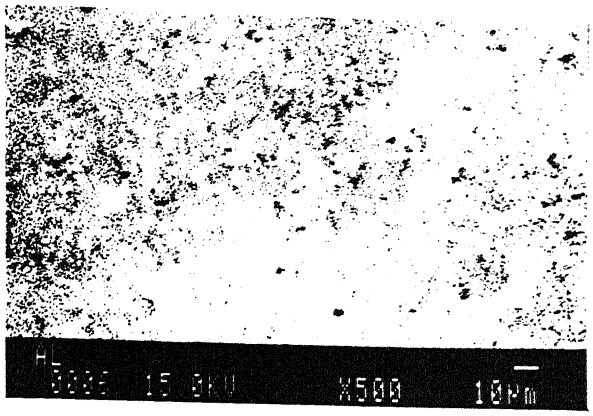

b

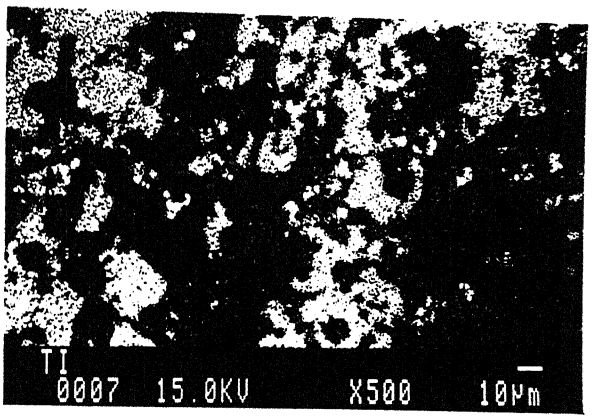

c

Fig.4.8 EPMA dot mapping of C4 sample (Al: TiO_2=1: 0.17 mole) heat treated for 7 hours at 1400 °C in vacuum. (a) Microstructure on which dot mapping was performed. (b) Dot map of aluminium (c) dot mapping of titanium. Mapping shows the uniform distribution of alumina and aluminides.

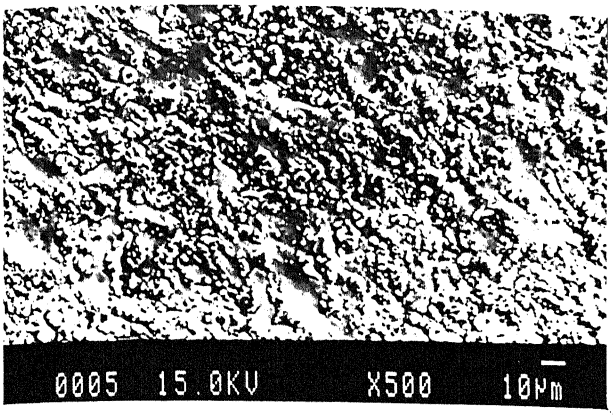

a

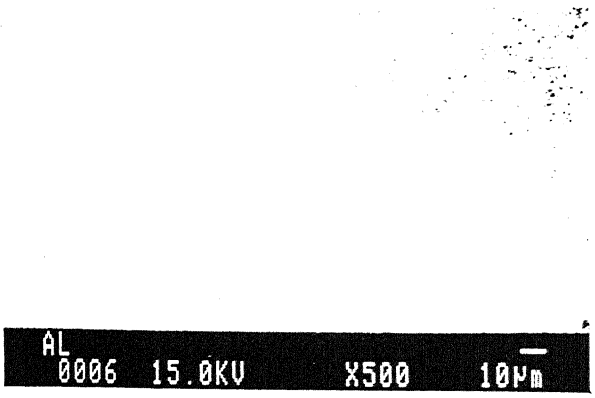

b

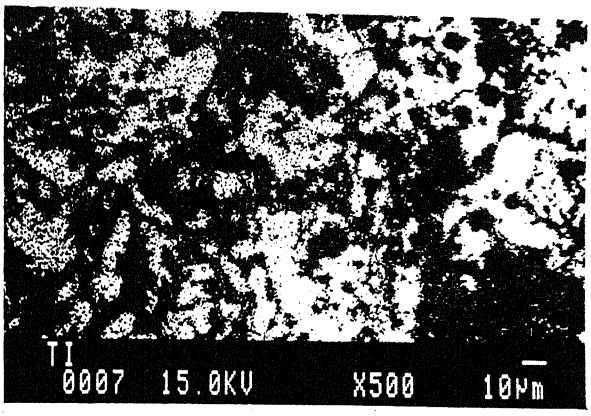

c

Fig.4.9 EPMA dot mapping of C4 sample (Al: TiO2=1: 0.156 mole) heat treated for 2 hours at 1400 °C in vacuum. (a) Microstructure on which dot mapping was performed. (b) dot map of aluminium (c) dot mapping of titanium. Mapping shows uniform distribution of alumina and aluminides.

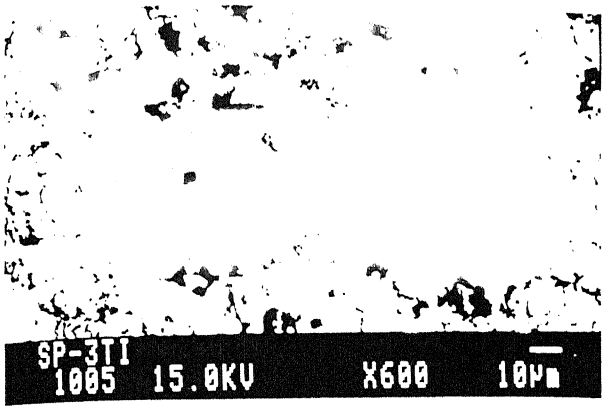

a

b

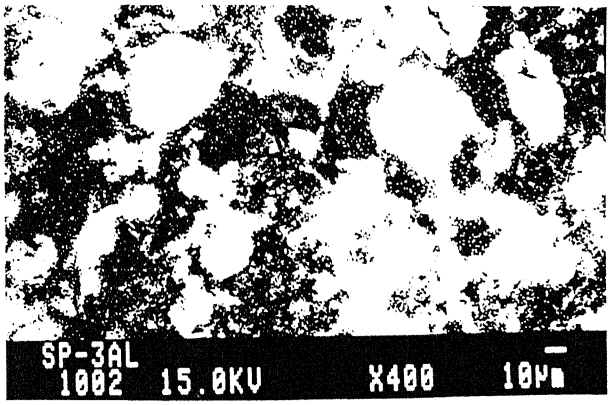

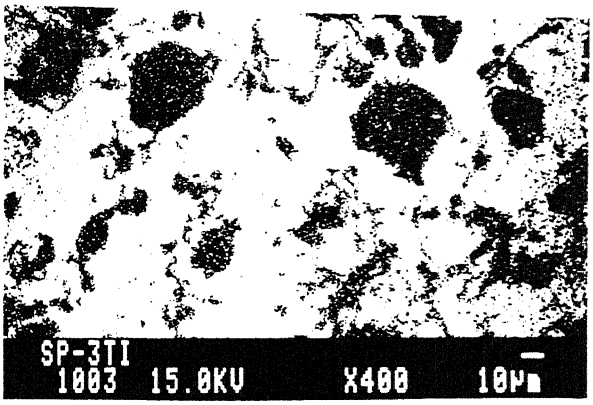

c

Fig.4.10 EPMA micrograph and dot mapping of C1 sample (Al: TiO_2=1: 0.56 mole) hot pressed at 800 °C. (a) shows the micrograph after hot pressing (b) Micrograph on which dot mapping was performed. (c) Dot map of aluminium (c) dot mapping of titanium. Mapping indicates incomplete reaction for this specimen. This could be because of lower aluminium content in the initial composition and insufficient time for reaction (since they are only hot pressed not heat treated).

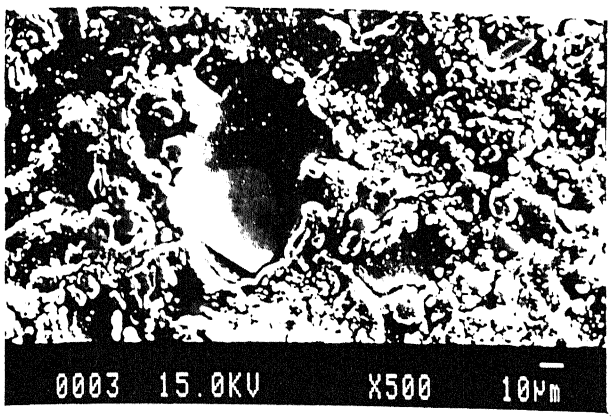

a

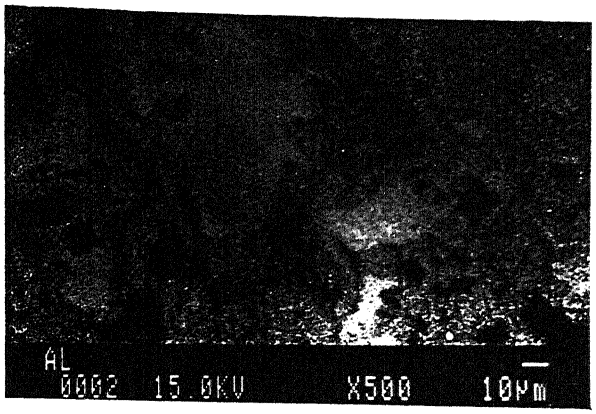

b

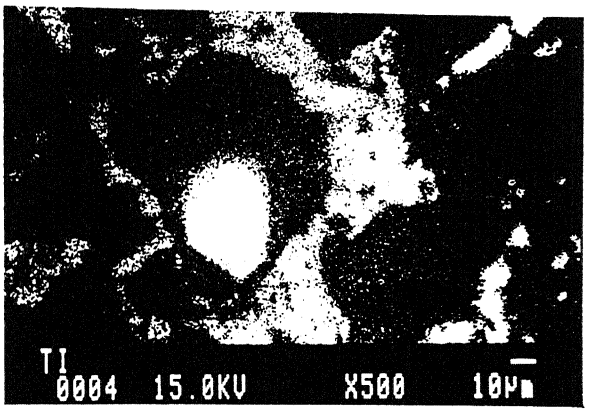

c

Fig. 4.11 EPMA dot mapping of green compacted sample (Al: TiO_2=1: 0.1184 mole) heat treated at 1400 °C in vacuum for 2hours. (a) Microstructure on which dot mapping was performed. (b) Dot map of aluminium (c) dot mapping of titanium. Mapping shows the uniform distribution of alumina and aluminides.

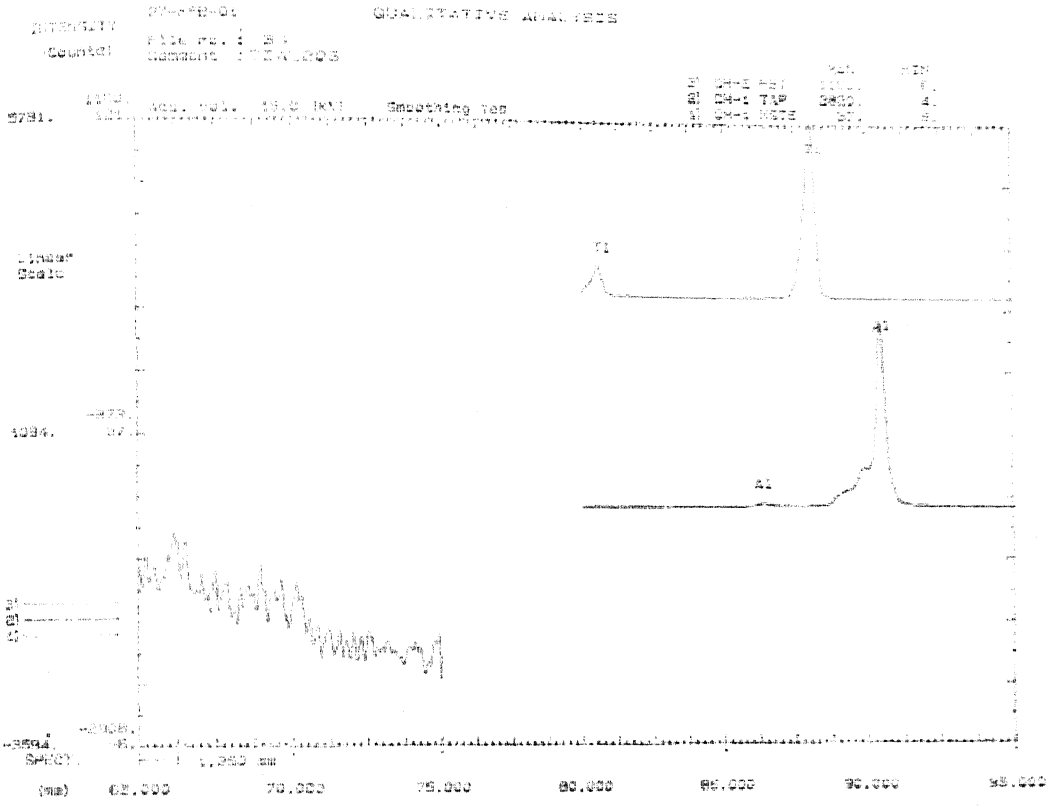

Fig. 4.12 Qualitative point analysis on aluminide phase.

Fig. 4.13 Qualitative point analysis on alumina phase.

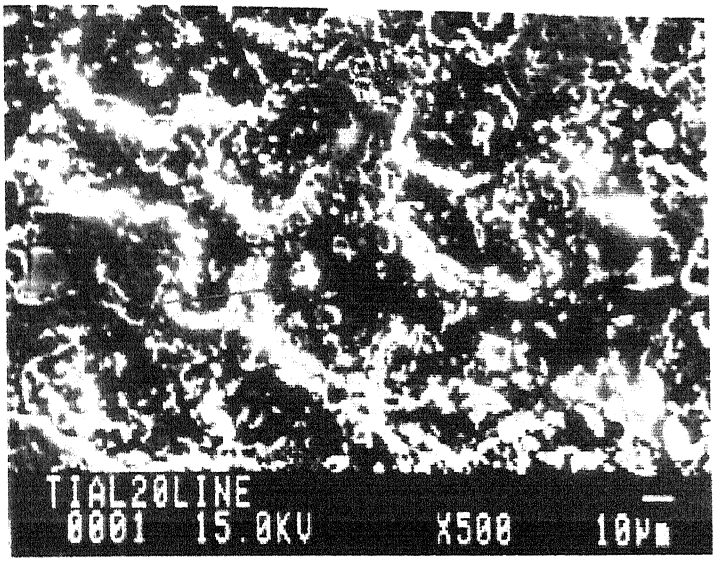

a

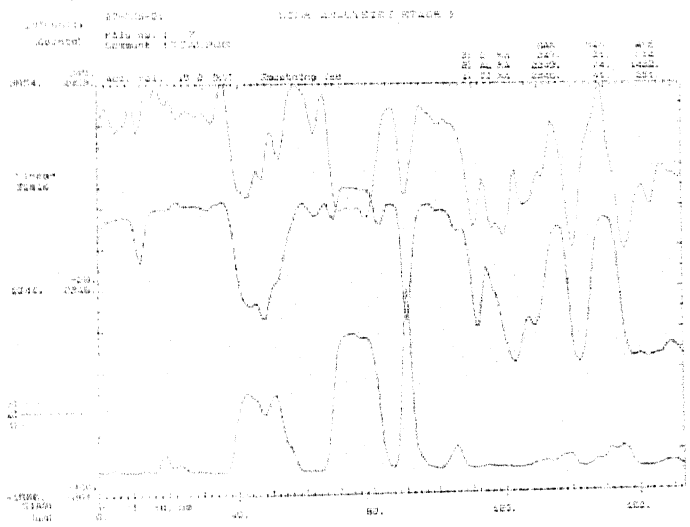

b

Fig.4.14 EPMA line analysis of the C3 sample (Al: TiO_2=1: 0.18 mole) heat treated for 1400 °C in vacuum. (a) Microstructure on which line analysis was performed. (b) Line analysis graph of aluminium and titanium.

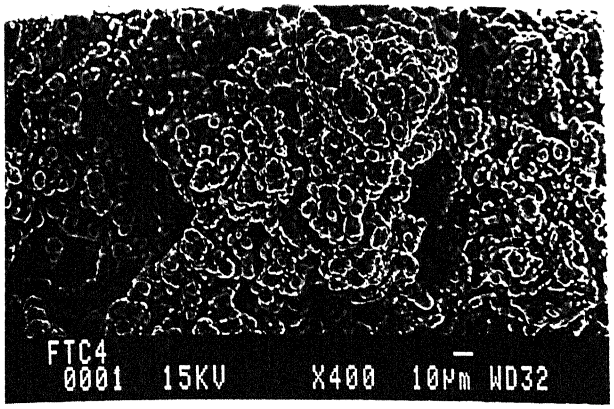

a

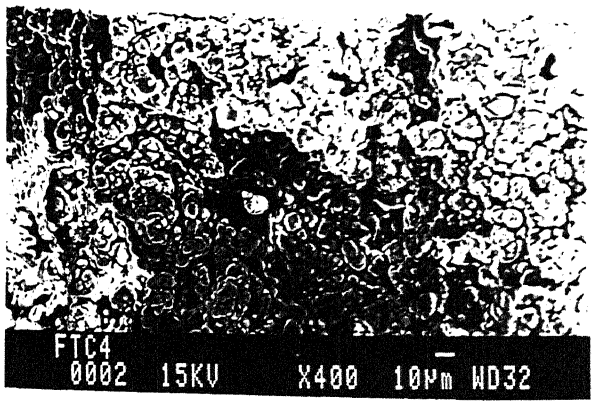

b

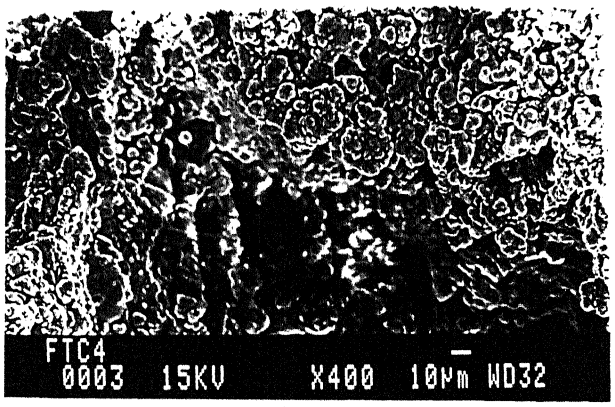

c

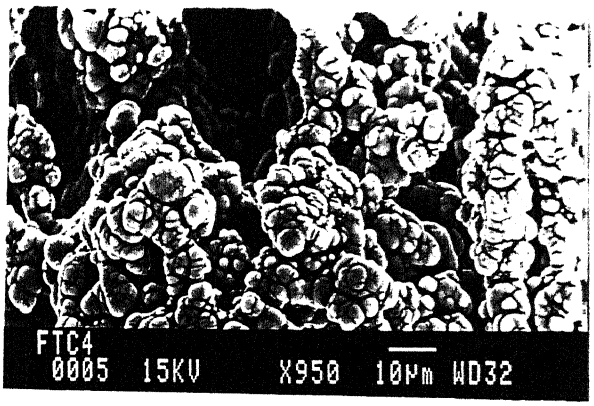

d

Fig. 4. 15 SEM micrographs showing the fracture path of a notched four point bent test (fracture toughness) sample PC4 (Al: TiO_2=1: 0.187 mole). (a), (b), (c) are fracture regions as we progressively move away from the notched surfaces. Crack path indicates the deflection of crack during the crack propagation. (d) Shows the presence of porosity in the sample and also crack deflection. It shows the separated black (Al_2O_3) particle.

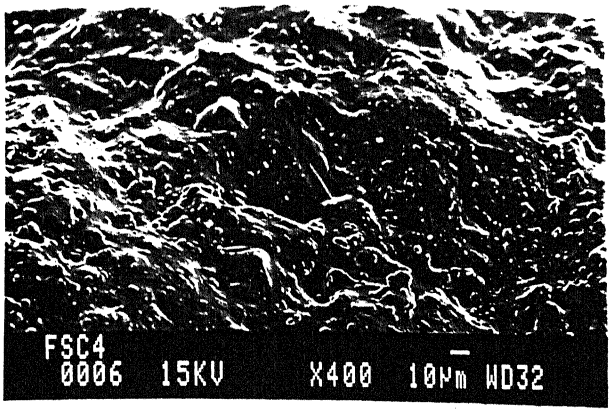

a

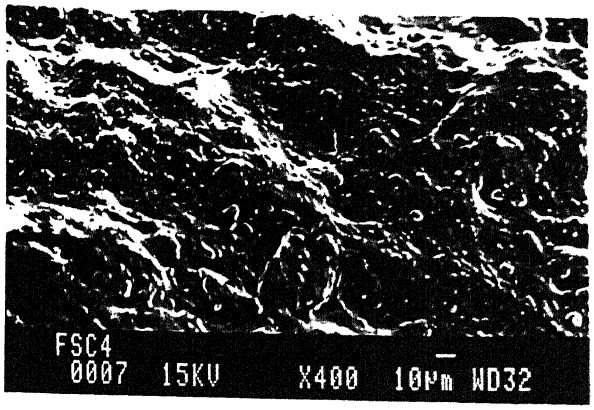

b

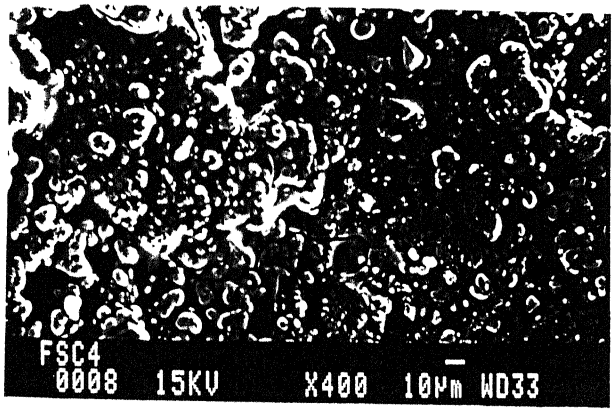

c

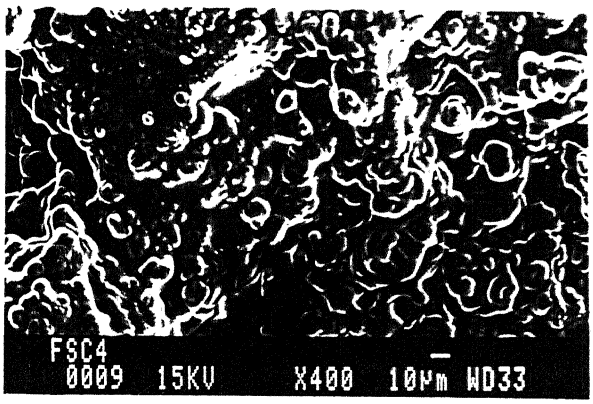

d

Fig. 4. 16 SEM micrographs showing the fractured surface of a un-notched four point bent test (flexural strength) sample PC4 (Al: TiO_2=1: 0.187 mole). (a) – (d) are from tensile end to the compressive end sequentially. (a) and (b) shows hills and valleys where as (c) and (d) indicates the crack deflection. (c) Shows matrix cracking.

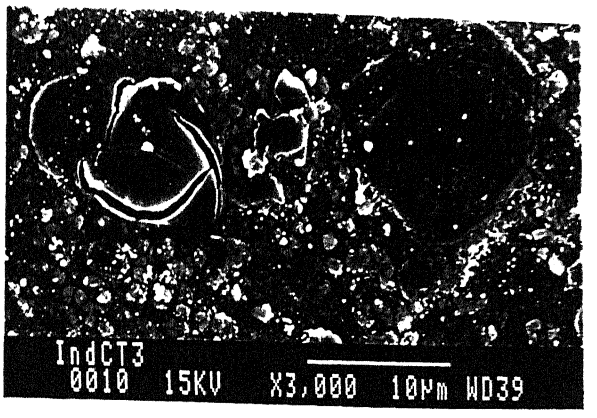

a

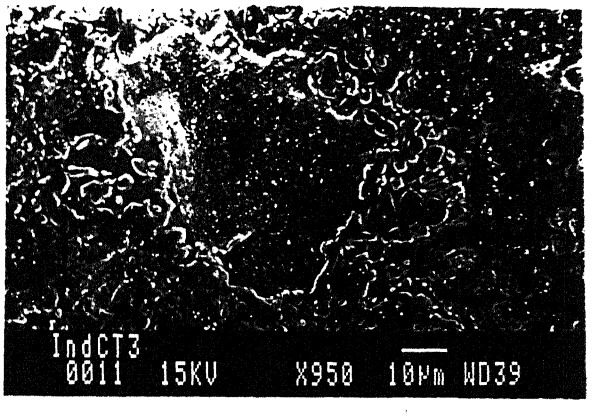

b

Fig. 4. 17 SEM micrographs showing the behavior indentation made using micro-hardness tester on PCT3 sample (Al: TiO_2 : Ti=1: 0.199 : 0.128 mole). (a) shows the fracture of grey phase(aluminide). Another indentation adjacent to it(right) reveals relatively softer material but no evidence of cracks. (b) Shows indentation made on the structure of aluminide and alumina.

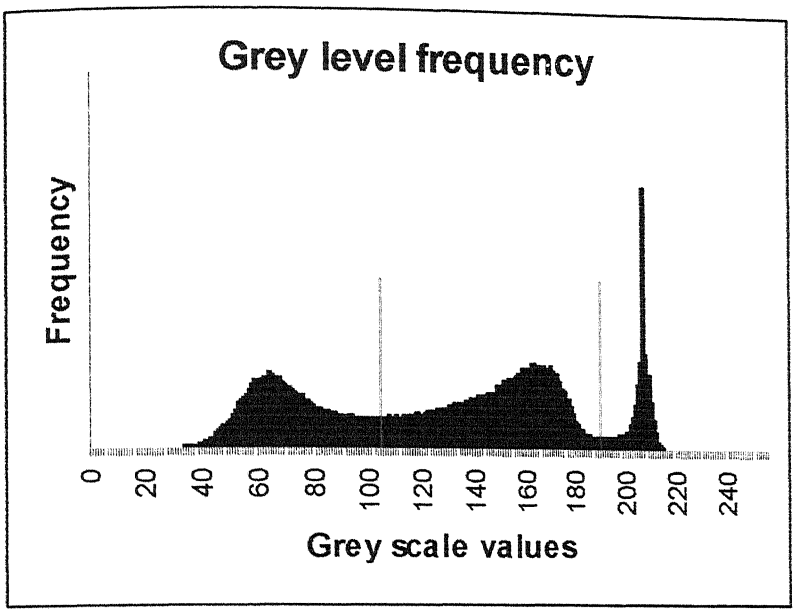

Fig.4.18 Histogram of the microstructure.

a

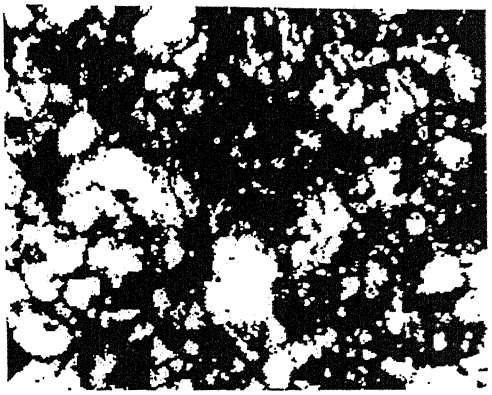

b

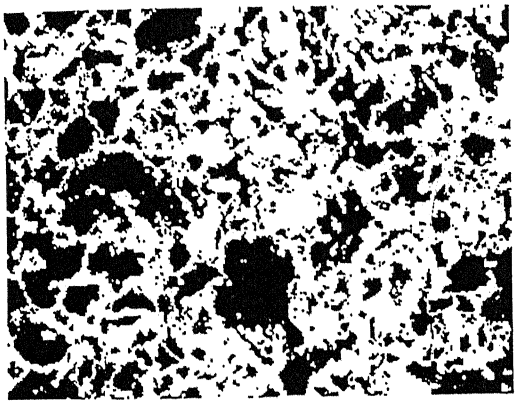

c

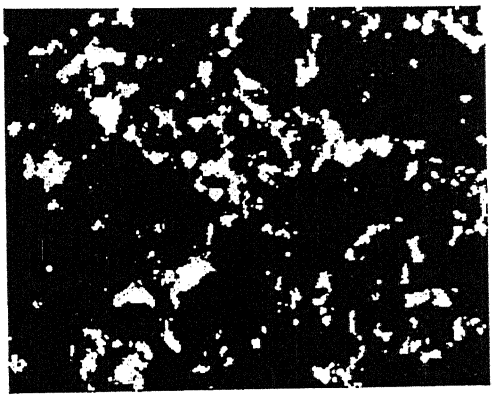

d

Fig.4.19 Microstructure on which Image processing was performed. (a) Microstructure of the sample containing three phases (b) black phase (c) gray phase (d) White phase.

REFERENCES

1. K.K.Chawla, 'Composite materials: science and engineering', Springer-Verlag, New York, U.S.A. (1987).
2. K.K.Chawla,' Ceramic matrix composites', University Press, Cambridge, U.K. (1993).
3. B.S.S. Daniel, V.S.R. Murthy, G.S. Murty, Metal matrix Composites via in situ methods, J. Mater. Proc. Tech., V.68, 1997, 132-155.
4. S.C.Tjong, Z.Y.Ma, Microstructural and mechanical characteristics of in situ metal matrix composites, Mater. Sci. and Engg A., V.29, 2000, 49-113.
5. S.Benerjee, S.K.Roy, Net-shape forming of bi-continuous Al_2O_3 /Al composite by displacement reaction, Mater. Chem. Phys., V.67, 2001, 243-248.
6. M. Hoffman, H. Mullejans, J.Rodel, S. Skirl, A. Zimmermann, E. Fuller, " Tailoring Of an interpenetrating network ceramic/metal microstructure to improve strength: Al_2O_3/Ni_3Al and Al_2O_3/Al, Novel synthesis and processing of ceramics, Kurume, Japan, 1997, Published in Key Engg. Mater. V.159-160,1999, 311-318.
7. V.S.R. Murthy, B.S.Rao, Microstructural development in the directed melt oxidized (DIMOX) Al-Mg-Si Alloys, J. Mater. Sci., V.30, 1995, 3091-3097.
8. B.S.S. Daniel, Processing and characterization of AlN/ Al base composites via directed metal nitridation, Ph.D. Thesis, I.I.T. Kanpur, July 1997.
9. B.S.S. Daniel, V.S.R. Murthy, Directed melt oxidation and nitridation of aluminum alloys: a comparision, Materials & Design, V.16, 1995, 155-161.
10. V.S.R. Murthy and A.Deepak, Microstructure and mechanical properties of SiC-Al_2O_3 composites prepared by directed melt infiltration, Brit. Ceram. Trans., V.95, 1996, 173-176.
11. Z.A. Munir, Synthesis of high temperature materials by self-propagating combustion methods, Am. Ceram. Soc. Bull., V.67, 1988, 342-349.
12. J.J. Moore and H.J. Feng, Combustion synthesis of advanced materials: Part I. reaction parameters, Prog. Mater. Sci., V.39,1995, 243-273.
13. J.J. Moore, H.J.Feng, Combustion synthesis of advanced materials: classification, applications and modeling, Prog. Mater. Sci., V.39, 1995, 275-316.

14. S. Schicker, D.E. Garcia, J. Bruhn, R. Janssen, and N. Claussen, Reaction synthesized Al_2O_3-based intermetallic composites, Acta. Mater., V.46, 1998, 2485-2492.

15. S. P. Gaus, M. P. Harmer, H. M. Chan, H. S. Ceram, N. Claussen, Alumina-aluminide alloys (3A) technology: I, model development, J. Am. Ceram. Soc., V.83, 2000, 1599-1605.

16. K.Ishida, R.Kainuma, N. Ueno and T.Nishizawa, Ductility enhancement in NiAl (B2)-base alloys by microstructural control, Metall.Trans. A, V.22A, 1991, 441-446.

17. M. Dollar, S. Dymec, S.J. Hwang and P. Nash, The role of microstructure on strength and ductility of hot-extruded mechanically alloyed NiAl, Metall. Trans. A, V.24, 1993, 1993-2000.

18. M. Inoue, K. Saganuma, K. Niihara, Fracture mechanism of Ni_3Al alloys and their composites with ceramic particles at elevated temperatures, Intermetallics, V.8, 2000, 365-370.

19. Y.W. Kim and M. Dimiduk, Progress in the understanding of gamma titanium aluminides, JOM, V.43, 1991, 40-47.

20. F.H. Froes, Structural intermetallics, JOM, V.41, 1989, 6-7.

21. R.L. Fleischer and A.I. Taub, Selecting high-temperature structural intermetallic compounds: the materials science approach, JOM, V.41, 1989, 8-11.

22. D.L. Anton, D.M. Shah, D.N. Dulh and F.H. Giamei, Selecting high-temperature structural intermetallic compounds: the engineering approach, JOM, V.41, 1989, 12-17.

23. C. Bassai, J.A. Peters and J. Wittenauer, Processing titanium aluminide foils, JOM, V.41, 1989, 18-20.

24. Y.W. Kim, Ordered intermetallic alloys, Part III: gamma titanium aluminides, JOM, V.46, 1994, 30-39.

25. D.E. Larsen, Y. Christodoulou, S.L. Kampe, and P. saldler, Investment-cast processing of XD^{TM} near-γ titanium aluminides, Mater. Sci. Engg. V.A144, 1991, 45-49.

26. B. A. Greenberg, M.A. Ivanov, New concepts of analyzing plastic deformation of TiAl and Ni_3Al intermetallic compounds, Mater. Sci. Engg. V.A153, 1992, 356-363.

27. D.A. Koss, D. Benerjee, D.A. Lukasak and A.K. Gogia, A review of the deformation and fracture of Ti_3Al based alloys, In high temperature aluminides & intermetallics, eds.S.H. Whang, C.T. Liu, D.P. Pope, and J.O. Stiegler, TMS, U.S.A (1990), 175-196.

28. S. Lee, J. Lee, Y. Lee, D.H. Shin and Y. Kim, Effect of heating rate on the combustion synthesis of intermetallics, Mater. Sci. Engg. A, V.A281, 2000, 275-285.

29. S.C. Tjong and Z.Y.Ma, Microstructural and mechanical characteristics of in situ metal matrix composites, Mater. Sci. and Engg., V.29, 2000, 49-113.

30. H.C. Yi and J.J. Moore, Self propagating high tempetature (combustion) synthesis (SHS) of powder-compacted materials, J.Mater.Sci., V.25, 1990, 1159-1168.

31. C.R. Bowen and B.Derby, Self propagating high temperature synthesis of ceramic materials, Brit. Ceram. Trans., V.96, 1996, 25-31.

32. R. Pampuch, Some fundamental versus practical aspects of self propagating high temperature synthesis, Solid State Ionics, V.101-103, 1997, 897-907.

33. A.G. Merzhanov in 'Combustion and plasma synthesis of high-temperature Materials, (Eds.) Z.A. Munir and J.B. Holt, VCH publishers, Weinheim, New york, 1990, P1.

34. Z.A. Munir and U. Anselmi-tamburini, Mater. Sci. Reprorts, V.3, 1989, 277-365.

35. J.W. McCauley, Historical and technical perspective on SHS, Ceram. Engg. Sci. Proc., V.11, 1990, 1137-1181.

36. K.A. Philpot, Z.A. Munir and J.B. Holt, An Investigation of the synthesis of nickel aluminides through gasless combustions, J. Mater. Sci. V.22, 1987, 159-169.

37. J.P. Lebrat, A. Verma, and A.E. Miller, Combustion synthesis of Ni_3Al and NiAl-Matrix composites, Metall. Trans A., V.23A, 1992, 69-76.

38. Y.Choi, M.E.Mullins, K.Wijayatillake and J.K. Lee, Fabrication of metal matrix Composites of TiC-Al through self propagating synthesis reaction, Metall.Trans.A, V.23A, 1992, 2387-2392.

39. S. Nourbakhsh and H. Margolin, Processing of continuous-ceramic-fiber-reinforced intermetallic composites by pressure casting, Mater. Sci. Engg. V.A144, 1991, 133-141.

40. H.J.Feng, J.J.Moore and D.G. Wirth, Combustion synthesis of ceramic-metal composite materials: the TiC-Al_2O_3-Al, Metall.Trans.A, V.23A, 1992, 2373-2379.

41. Z.A.Munir, The preparation of multiphase materials through self sustaining powder reactions, In sintering of multiphase metal and ceramic systems, ed. G.S.Upadhyaya, Sci-Tech publication , U.S.A. (1990), 37-46.

42. C. Subramanyan and M. Vijaykumar, Self propagating high temperature synthesis, J. Mater. Sci., V.27, 1992, 6249-6273.

43. V.I. Itin, A.D. Bratchikov and L.N. Postnikova, Use of combustion and thermal explosion for the synthesis of intermetallic compounds and their alloys, Sov. Powd. Met. Ceram, V5(209), 1980, 315-318.

44. R. Subramanian, C. G. McKamey, J. H. Schneibel, L. R. Buck and P. A. Menchhofer, Iron aluminide-Al_2O_3 composites by in situ displacement reactions: processing and mechanical properties, , Mater. Sci. Engg A, V.A1254, 1998, 119-128.

45. R. Subramanian, C. G. McKamey, L. R. Buck and J. H. Schneibel, Synthesis of iron aluminide-Al_2O_3 Composites by in-situ displacement reactions, Mater. Sci. Engg A, V.A239-240, 1997, 640-646.

46. O.N. Senkov, M. Cavusoglu, F.H. Froes, Synthesis and characterization of a TiAl/Ti_5Al_3 composite with a submicrocrystalline structure, Mater. Sci. Engg, V.A300, 2001, 85-93.

47. D.K. Mukhopadhyay and F.H. Froes, Synthesis of Ti aluminides using a combined mechanical alloying and thermo hydrogen processing approach, Advanced Particulate Materials and Processes, MPIF, Princeton, New Jersy, USA., 1997, 145-152.

48. C.M. Ward-Close, P.S. Goodwin, M.L. Ovecoglu and F.H. Froes, Microstructural control in γ-TiAl intermetallic powder compacts, Advanced Particulate Materials and Processes, MPIF, Princeton, New Jersy, USA., 1997, 139-144.

49. K.P. Rao and Y.J. Du, In situ formation of titanium silicides-reinforced TiAl-based composites, Mat. Sci. Engg. A., V. 277, 2000, 46-56.

50. R. Orru, G. Cao and Z.A. Munir, Field-activated combustion synthesis of titanium aluminides, Met. Trans. A, V.30, 1999, 1101-1108.

51. T. Matsubara, S. Morino, K. Uenishi and K.F. Kobayashi, Fabrication of Al_3Ti layer on Cu substrate by SHS reaction of mechanically alloyed powder, J. Soc.Mater. Sci., Japan, V. 47, 1998, 1106-1111.

52. F. Appel and R. Wagner, Microstructure and deformation of two phase γ titanium aluminides, Mater. Sci. and Engg.R, V.R 22, 1998,187- 268.

53. T.T.Cheng, The mechanism of grain refinement in TiAl alloys by boron addition- an alternative hypothesis, Intermetallics, V.8, 2000, 29-37.

54. Y. Choi, M.E. Mullins, K. Wijayatillake and J.K. Lee, Fabrication of metal matrix composites of TiC-Al through self propagating synthesis reaction, Metall. Trans.A, V. 23A, 1992, 2387-2392.H.P. Li, S.B. Bhaduri and J.A. Sekhar, Metal ceramic composites based on the Ti-B-Cu porosity system, Metall.Trans.A, V.23A, 1992, 251-261.

55. H.P. Li, S.B. Bhaduri and J.A. Sekhar, Metal ceramic composites based on the Ti-B-cu porosity system , Metall. Trans.A, V23A, 1992, 251-261.

56. H.J. Feng, J.J. Moore and D.G. Wirth, Combustion synthesis of ceramic-metal composite materials:The TiC-Al_2O_3-Al, Metall.Trans.A, V.23A,1992, 2373-2379.

57. R. Orru, G. Cao and Z.A. Munir, Field activated combustion synthesis of titanium aluminides, Met. and Mater.Trans. A, V. 30, 1999, 1101-1108.

58. D.E. Garcia, S.Schicker, J. Bruhn, A. Krupp, R. Janssen and N. Claussen, Al_2O_3 containing Fe, Nb and Zr aluminides, High Temp. Ord. Intermetallics Alloys VII; Mater. Res. Soc. Symp. Proc., V.460, 1997, 761-766.

59. B. K. Yen, T. Aizawa, J. Kihara, Synthesis and formation mechanisms of molybdenum silicides by mechanicai alloying, Mater. Sci. and Engg. V. A220, 1996, 8-14.

60. C.H. Gras, F. Charlot, E. Gaffet, F. Bernard and J.C. Niepce, In situ synchrotron characterization of mechanically activated self propagating high temperature synthesis applied in Mo-Si system, Acta. Mater, .47 (1999) 2113-2123.

61. P. Pampuch, J.Lis and L. Stobierski, in 'Combustion and plasma synthesis of high-temperature materials', (Eds.) Z.A. Munir and J.B. Holt, VCH Publishres, Weinham, New York, 1990, P211.

62. S. Schicker, D.E. Garcia, I. Gorlov, R. Janssen and N. Claussen, Wet milling of Fe_2O_3/Al/ Al_2O_3 powder mixtures, J. Am. Ceram. Soc., V.82, 1999, 2607-2612.

63. J. Bruhn, S. Scicker, D.E. Garcia, R. Janssen, F. Wagner and N. Claussen, Novel reaction-based processing of co-continuous ceramic-metal composites, Key. Engg. Mater, V.127-131, 1997, 73-80.

64. C. Scheu, D. Dehm, W. D. Kaplon, Microstructure of alumina composites containing niobium and niobium aluminides, J. Am. Ceram. Soc., V.83, 397-402, 2000.

65. D. E. Garcia, S. Schicker, J. Bruhn, R. Janssen and N. Claussen, Synthesis of novel niobium based composites, J. Am. Ceram. Soc., V.80, 1997, 2248-2252.

66. S. P. Gaus, M. P. Harmer, H. M. Chan, H. S. Ceram and N. Claussen, Alumina-Aluminide Alloys (3A) technology: II, modelling of Ti_xAl_y-Al_2O_3 composite formation, J. Am. Ceram. Soc., V.83, 2000, 1606-1612.

67. J. Rödel, H. Prielipp, N. Claussen, M. Sternitzke, K.B. Alexander, P.F. Becher, and J.H. Schneibel, Ni_3Al/Al_2O_3 composites with interpenetrating networks, Scripta Metallurgica, V.33, 1995, 843-848.

68. F. Wagner, D.E. Garcia, A. Krupp and N. Claussen, Interpenetrating Al_2O_3-$TiAl_3$ alloys produced by reactive infiltration, J. Eu. Ceram. Soc.,V. 19, 1999, 2449-2453.

69. S. Schicker, T. Erny, D.E. Garcia, R. Janssen and N. Claussen, Microstructure and mechanical properties of Al-assisted sintered Fe/Al_2O_3 cermets, J. Eu. Ceram. Soc., V.19, 1999, 2455-2463.

70. C. F. Feng, L. Froyen, Formation of Al_3Ti and Al-TiO_2 system for preparing in situ alumina composites, Composites: Part A , V.31, 2000, 385-390.

71. W.G. Fahrenholtz, K.G. Ewsuk, R.E. Loehman and A.P. Tomsia, Formation of structural intermetallics by reactive metal penetration of Ti and Ni oxides and aluminides, Metall. Mater. Trans. A, V.27A, 1996, 2100-2104.

72. N. Claussen, D.E. Garcia and R. Janssen, Reaction sintering of Alumina-Aluminide Alloys (3A), J. Mater. Res., V.11, 1996, 2884-2888.

73. N. Claussen, J. Bruhn, D.E. Garcia, R. Janssen and S. Schicker, Intermetallics reinforced alumina, Ceram. Engg. Sci. Proc. , V.15, 1994, 395-399.

74. D.E. Garcia, J. Bruhn, S. Schicker, R. Janssen and N. Claussen, Alumina-Aluminide Alloys (3A), Ceram. Trans., V.79, 1996, 219-221.

75. S. Schicker, D.E. Garcia, J. Bruhn, R. Janssen and N. Claussen, Reaction processing of Al_2O_3 composites containing iron and iron aluminides, J. Am. Ceram. Soc., V.80, 1997, 2294-2300.

76. R.C. Weast, Handbook of chemistry and physics, 55^{th} edition, CRC Press, Cleveland, 1974, D-58.

77. H.X. Zhu, R. Abbaschian, In situ processing of NiAl-alumina composites by thermit reaction, Mater. Sci. Engg. A, V.A282, 2000, 1-7.

78. M.R. Ghomashchi, Fabrication of near net shaped Al-based intermetallic matrix composites, J. Mater. Process. Technol, V.112, 2001, 227-235.

79. C.K. Lin, S.S. Hong, P.W. Lee, Formation of NiAl-Al_2O_3 intermetallic matrix composite powders by mechanical alloying technique, Intermetallics, V.8, 2000, 1043-1048.

80. C. Scheu, D. Dehm and W. D. Kaplon, Microstructure of alumina composites containing niobium and niobium aluminides, J. Am. Ceram. Soc., V.83, 2000, 397-402.

81. B.S. Murthy and S. Ranganathan, Novel materials synthesis by mechanical alloying/ milling, Inter. Mater. Rev., V.43, 1998, 101-141.

82. C. Suryanarayana, Mechanical alloying and milling, Prog. Mater. Sci., V.46, 2001, 1-184.

83. K.B. Gerasimov, A.A. Gusev, E.Y.Ivanov and E.E. Boldyrev, Tribochemical equilibrium in mechanically alloyed metals, J. Mater. Sci., V.26, 1991, 2495-2500.

84. W. Guo, A. Isonna, M. Magini, S. Martelli, F. Pedella, Synthesis of amorphous and metastable Ti40-Al60 alloys by mechanical alloying of elemental powders, J. Mater.Sci., V.29, 1994, 2436-2444.

85. M.S. El Eskandarany, Thermally assisted and mechanically driven solid state reactions for formations of amorphous $Al_{33}Ta_{67}$ alloy powders, Metall. Mater. Trans., V. A27, 1996, 3267-3278.

86. H.C. Yi, A. Petric and J.J. Moore, Effect of heating rate on the combustion synthesis of Ti-Al intermetallic compounds, J. Mater. Sci., V.27, 1992, 6797-6806.

87. J. Karch, R. Birringer and H. Gleiter, Ceramics ductile at low temperature, Nature, V.330, 1987, 556-558.

88. G.H. Chen, C. Suryanarayana and F.H. Froes, Synthesis of B2 Phase in Ti-Al-Nb alloys by mechanical alloying, Scripta metal. Mater., V.25, 1991, 2537-2540.

89. R. Lerf, D.G. Morries, Mechanical alloying of Al-Ti alloys, Mater. Sci. Engg A, V.A128, 1990, 119-127.

90. A. Hellwig, G. Inden, and M. Palm, The invariant reaction between α, α_2 and γ in the Ti-Al system, Scrip. Metall. Mater., V.27, 1992, 143-148.

91. C. H. Gras, F. Charlot, E. Gaffet, F. Bernard and J.C. Niepce, In situ synchrotron characterization of mechanically activated self propagating high temperature synthesis applied in Mo-Si system, Acta. Mater, V.47, 1999, 2113-2123.

92. Y.M. Kim, Intermetallics alloys based on gamma-titanium aluminides, JOM, V.41, 1989, 24-30.

93. F.H.Froes, C. Suryanarayana and D. Eliezer, Production, characteristics, and commercialization of titanium aluminides, ISIJ International, V.31,1991, 1235-1248.

94. D.M. Dimiduk, D.B. Miracle, Y.W. Kim and M.G. Mendiratta, Recent progress on intermetallic alloys for advanced aerospace systems, ISIJ International, V.31, 1991, 1223-1234.

95. F.H. Froes, C. Suryanarayana, D. Eliezer, Synthesis, properties and applications of titanium aluminides, J. Mater. Sci., V.27, 1992, 5113-5140.

96. Y.Fu, R. Shi, J. Zhang, J. Sun, G. Hu, Microstructure and mechanical behavior of a multiphase Al_3Ti-based intermetallic alloy, Intermetallics, V.8, 2000, 1251-1256.

97. S. Srinivasan, P.B. Desch and R.B.Schwarz, Metastable phases in the Al_3X (X+Ti,Zr,Hf) intermetallic system, Scri. Metall, V.25, 1991, 2513-2616.

98. M.Atzmon, In situ thermal observation of explosive compound formation reaction during mechanical alloying, Phy. Rev. Lett., V.64, 1990, 487-490.

99. H. Schropf, C. Kuhrt, E. Arzt and L. Schultz, Ordering versus disordering tendencies in mechanically alloyed (Ni_XFe_{1-X}) Al alloys, Scri. Metall. Mater., V.30, 1994, 1569- 1574.

100. J.S.C. Jang and C.C. Koch, Amorphisation and disordering of the Ni_3Al ordered Intermetalic by mecahanical alloying, J. Mater. Res., V.5, 1990, 498-510.

101. S.W .Chae, C.H. Son, Y.S. Kim, Finite element analysis on the effect of silicon phase melting in combustion synthesis of $MoSi_2$, Mater Sci. Engg. V.279, 2000, 111-117.

102. L. Liu and M. Magini, Correlation between energy transfers and solid state reaction induced by mechanical alloying on the Mo-Si system, J. Mater. Res.,V.12 1997, 2281-2287.

103. C.H. Gras,. E. Gaffet, F. Bernard, F. Charlot and J.C. Niepse, Mechanically activated self propagating high temperature synthesis (MASHS) applied to $MoSi_2$ and $FeSi_2$ phase formation, Mater. Sci. For., V.312, 1999, 287-292.

104. .F. Charlot, E. Gaffet, F. Bernard, C.H. Gras and J.C. Niepse, Nanocrystalline FeA synthesis by MASHS with in situ and post mortem characterizations, Mater. Sci. Form., V.312, 1999, 287-292.

105. F.Charlot, E.Gaffet, B.Zaghmati, F.Bernard and J.C.Niepse, Mechanically activated synthesis by x-ray diffraction in the Fe-Al system, Mater. Sci. Engg A V.262, 1999, 297-288.

106. F. Charlot, F. Bernard, E. Gaffet, D. Clain, D. Klein and J.C. Niepse, In situ time resolved diffraction coupled with an i.r. camera to study mechanically activated SHS reaction : case of Fe-Al systems, Acta. Mater. V.47, 1999, 619-629.

107. B.H. Robin and R.N. Wright, Synthesis of iron aluminides from elemental Powders: reaction mechanism and densification behavior, Met. Trans A, V.22A, 1991, 277-286.

108. V. Gothier, F. Bernard, E. Gaffet, C. Josse and J.P. Larpin, In situ time resolved x-ray diffraction study of the formation of the nanocrystalline $NbAl_3$ phase by

mechanically activated self propagating high temperature synthesis reaction, Mater. Sci. Engg A, V. 272, 1999, 334-341.

109. B. Li, L. Rong, V.E. Gjunter and Y. Li, Porous Ni_Ti shape memory alloys produced by two different methods, Mater. Res. Adv. Techn., V 91, 2000, 291-295.

110. F.M.H. Zarandi and K.Sadrnezhaad, Thermochanical study of combustion synthesized Ti-Ni shape memory alloy, Mater. Manuf. Proc., V.12, 1997, 1093-1105.

111. H.P. Yi and J.J. Moore, Combustion synthesis of TiNi intermetallic compounds, Part I, determination of heat of fusion of TiNi and heat capacity of TiNi, J. Mater. Sci., V. 24, 1989, 3449-3456.

112. H.P. Yi and J.J. Moore, Combustion synthesis of TiNi intermetallic compounds, Part 2, effect of TiO_2 formation, J. Mater. Sci. V.24, 1989, 3457-3462.

113. W.G. Fahrenholtz, K.G. Ewsuk, R.E. Loehman and A.P. Tomsia, Formation of structural intermetallics by reactive metal penetration of Ti and Ni oxides and aluminides, Metall. Mater. Trans.A, V.27A, 1996, 2100-2104.

114. F.H. Froes, C. Suryanarayana and D. Eliezer, Synthesis, properties and applications of titanium aluminides, J. Mater. Sci. V.27, 1992, 5113-5140.

115. R.M. Imayev, M.K. Gabdullin, G.A. Salishchev, O.N. Senkov, V.M. Imayev, and F.H. Froes, Efecct of grain size and partial disordering on ductility of Ti_3Al in the temperature range of 20°-600°C, Acta Mater. V.47, 1999, 1807-1821.

116. R.J. Laderich, J.L. McAfee and D.S. Schwartz, Superplastic forming and the resulting mechanical properties of Ti-14wt%Al-20wt% Nb-3.2wt%V-2wt%Mo, Mater. Sci. Engg. A, V.A189, 1994, 29-33.

117. V.M. Imayev, R.M. Imayev, G.A. Salishchev, K.B. Pavarova, M.R. Shagiev and A.V. Kuznetsov, Effect of strain rate on twinning and room temperature ductility of TiAl with fine equiaxed microstructure, Scri. Mater., V.36, 1997, 891-897.

118. T. Kawabata and O. Izumi, Recent mechanical properties of TiAl, In high temperature aluminides & intermetaliics, eds.S.H. Whang, C.T. Liu, D.P. Pope, and J.O. Stiegler, TMS, U.S.A(1990), 403-424.

mechanically activated self propagating high temperature synthesis reaction, Mater. Sci. Engg A, V. 272, 1999, 334-341.

109. B. Li, L. Rong, V.E. Gjunter and Y. Li, Porous Ni_Ti shape memory alloys produced by two different methods, Mater. Res. Adv. Techn., V 91, 2000, 291-295.

110. F.M.H. Zarandi and K.Sadrnezhaad, Thermochanical study of combustion synthesized Ti-Ni shape memory alloy, Mater. Manuf. Proc., V.12, 1997, 1093-1105.

111. H.P. Yi and J.J. Moore, Combustion synthesis of TiNi intermetallic compounds, Part I, determination of heat of fusion of TiNi and heat capacity of TiNi, J. Mater. Sci., V. 24, 1989, 3449-3456.

112. H.P. Yi and J.J. Moore, Combustion synthesis of TiNi intermetallic compounds, Part 2, effect of TiO_2 formation, J. Mater. Sci. V.24, 1989, 3457-3462.

113. W.G. Fahrenholtz, K.G. Ewsuk, R.E. Loehman and A.P. Tomsia, Formation of structural intermetallics by reactive metal penetration of Ti and Ni oxides and aluminides, Metall. Mater. Trans.A, V.27A, 1996, 2100-2104.

114. F.H. Froes, C. Suryanarayana and D. Eliezer, Synthesis, properties and applications of titanium aluminides, J. Mater. Sci. V.27, 1992, 5113-5140.

115. R.M. Imayev, M.K. Gabdullin, G.A. Salishchev, O.N. Senkov, V.M. Imayev, and F.H. Froes, Efecct of grain size and partial disordering on ductility of Ti_3Al in the temperature range of 20°-600°C, Acta Mater. V.47, 1999, 1807-1821.

116. R.J. Laderich, J.L. McAfee and D.S. Schwartz, Superplastic forming and the resulting mechanical properties of Ti-14wt%Al-20wt% Nb-3.2wt%V-2wt%Mo, Mater. Sci. Engg. A, V.A189, 1994, 29-33.

117. V.M. Imayev, R.M. Imayev, G.A. Salishchev, K.B. Pavarova, M.R. Shagiev and A.V. Kuznetsov, Effect of strain rate on twinning and room temperature ductility of TiAl with fine equiaxed microstructure, Scri. Mater., V.36, 1997, 891-897.

118. T. Kawabata and O. Izumi, Recent mechanical properties of TiAl, In high temperature aluminides & intermetaliics, eds.S.H. Whang, C.T. Liu, D.P. Pope, and J.O. Stiegler, TMS, U.S.A(1990), 403-424.

119. V.M. Imayev, R.M. Imayev and G.A. Salishchev, Porosity of TiAl intermetallic compound with micro and submicro crystalline structure after superplastic deformation, Mater. Sci. Engg. A V.A208, 1996, 226-231.

120. M.H. Loretto, D. Hu and Y.G. Li, Microstructural study on some ordered Ti-base alloys, Intermetallics, V.8, 2000, 1243-1249.

121. G. Sauthoff, Multiphase intermetallic alloys for structural applications, Intermetallics, V.8, 2000,1101-1109.

122. F.H. Froes, C. Suryanarayana and D. Eliezer, Production, characteristics, and commercialization of titanium aluminides, ISIJ Inter., V.31, 1991, 1235-1248.

123. A. Appel, P.A. Beaven, and R. Wagner, Deformation processes related to interfacial boundaries in two phases γ Titanium aluminides, Acta. Metall. Mater. V.41, 1993, 1721-1732.

124. L. Zhao and K. Tangri, TEM investigations on the interfacial boundaries in as cast Ti_3Al+TiAl Alloy, Acta. .Metall. Mater. V.39, 1991, 2209-2224.

125. K.S. Chan and Y.M. Kim, Influence of microstructure on crack tip micromechanics and fracture behaviors of a two-phase TiAl alloy, Met.Trans. A, V.23A, 1992, 1663-1667.

126. K.S. Chan and Y.M.Kim, Rate and environmental effects on fracture of a two-phase TiAl alloy, Met.Trans. A, V.24A, 1993, 113-125.

127. R. Gnanamoorthy, Y. Mutoh, N. Masahashi and Y. Mizuhara, Fracture properties of γ-base TiAl alloys with lamellar microstructure at room temperature, Mater. Sci. Engg, V. A184, 1994, 37-44.

128. W.O. Soboyejo, D.S. Schwartzand and S.M.L. Sastry, An investigation of the fracture behavior of the gamma-based titanium aluminides: effects of annealing in the α+γ and α_2+γ phase fields, Met. Trans A. V.23A, 1992, 2039-2059.

129. R. Gnanamoorthy, Y. Mutoh, N.Masahashi and Y.Mizuhara, Fracture toughness of gamma-base titanium aluminides, Met. Trans. V.26A, 1995, 305-313.

130. D.E. Albert, and A.W. Thompson, Effect of Microstructure on Creep of Ti-24Al-11Nb Polycrystals, Met. Trans A. V.23A, 1992, 3035-3043.

131. M. Matsuo, Developments in processing technology of gamma titanium aluminides for potential application to airframe structures, ISIJ International, V.31, 1991, 1212-1222.

132. V.M. Imayev, G.A. Salishchev, M.R. Shagiev, A.V. Kuznetsov, R.M. Imanev, O.N. Senkev and F.H. Froes, Low-temperature superplasticity of subcrystalline Ti-48Al-2Nb-2Cr alloy produced by multiple forging, Scri. Mater., V.40, 1999, 183-190.

133. P.J. Maziasz and C.T. Liu, Development of ultrafine lamellar structures in two-phase γ-TiAl alloys, Met. Trans A. V.29A, 1998, 105-117.

134. K. Hashimoto, M. Nibuki, T. Tsujimoto, and T.Suzuki, Deformation behaviour of TiAl base alloy containing manganese at elevated temperatures, ISIJ International, V.31, 1991, 1154-1160.

135. S.C. Huang, E.L. Hall and D.S. Shih, Microstructure and ductility of TiAl alloys modified by Cr additions, ISIJ Inter., V.31, 1991, 1100-1105.

136. M. Saqib, I. Weiss, G.M. Mehrotra, E. Cleavenger, A.G. Jackson, and H.A. Lipsitt, Microstructural and thermal Stability of a Ti-43Al alloy containing dispersoids of Titanium diboride, Met. Trans A. V.22A, 1991, 1721-1728.

137. S.L. Kampe, P. Sadler, L. Christodoulou, and D.E. Larsen, Room-temperature strength and deformation of TiB_2 reinforced near gamma titanium aluminides, Met. Trans A. V.25A, 1994, 2181-2197.

138. G.A. Salishchev, R.M. Imanev, O.N. Senkev, and F.H. Froes, Microstructural control in Ti-Al for enhanced mechanical properties, JOM, 2000, 46-48.

139. K.S. Chan, Toughning mechanisms in titanium aluminides, Met. Trans A. V.24A, 1993, 569-583.

140. K.W. Liu, R. Gerling and F.P. Schimansky, Microstructure and tensile properties of spray formed gamma Ti-48.9Al, Scri. Mater., V.40, 1999, 601-608.

141. F. Appel, M. Oehring, R. Wagner, Novel concept designs for gamma-base titanium aluminide alloys, Intermetallics, v.8, 2000, 1283-1312.

142. H. Moll, and B.J. McTiernan, P/M TiAl: the sky's the limit, MPR, V.55, 2000, 18-22.

143. J.J. Krusic, J.P. Campbell, and R.O. Ritchie, On the fatigue behaviour of γ-based titanium aluminides: roll of small cracks, Acta Mater, V.47, 1999, 801-816.

144. S.A. Bentley, A.L. Mantle, and D.K. Aspinwall, The effect of machining on the fatigue strength of a gamma titanium aluminide intermetallic alloy, Intermetallics, V.7, 1999, 967-969.

145. R. Gnanamoorthy, Y.Mutoh, K.Hayashi, and Y. Mizuhara, Influence of lamellar lath orientation on the fatigue crack growth behaviour of gamma base titanium aluminides, Scri. Metall. Mater., V.33, 1995, 907-912.

146. D.A. Wheeler, B. London and D.E. Larsen, Jr, Steady state creep deformation of investment cast near gamma titanium aluminide, Scripta Metall. Mater, V.26, 1992, 939-944.

147. N. Masahashi, Y. Mizuhara, M. Matsuo, T. Hanamura, M. Kimura and K.Hashimoto, High temperature deformation behaviour of titanium-aluminide based gamma plus beta microduplex alloy, ISIJ Inter., V..31, 1991, 728-737.

148. J. Beddoes, High temperature compression behavior of near gamma titanium aluminides containing additions of chromium or tungsten, Mater. Sci. Engg. A V.A184, 1994, L11-L15.

149. M. Dahms, J. Seeger, W. Smarley and B. Wildhagen, Titanium aluminides by hot isostatic pressing of cold extruded titanium-aluminium powder mixtures, ISIJ Inter., V.31, 1991, 1093-1099.

150. P.L. Sullivan, HIP Processing of Ti-Al Intermetallic using using blended elemental powders, J. Mater. Process. Technol, V.38, 1993, 1-14.

151. J. Bruhn, S. Schicker, D.E. Garcia, R. Janssen, F. Wagner and N. Claussen, Novel reaction-based processing of co-continuous ceramic-metal composites, Key. Engg. Mater, V.127-131, 1997, 73-80.

152. S.T. Mileiko, K.B. Povarova, V.P. Korzhov, A.V. Serebyyakov, A.A. Kolchin, V.M. Kiiko, M.Y. Starostin, N.S. Sarkissyan, and A.V. Antonova, High-temperature creep of sapphire-fibre/titanium-aluminide-matrix composites, Scri. Mater, V.44, 2001, 2463-2469.

153. G. Fanta, R. Bohn, M. Dahms, T. Klassen, R. Bormann, The effect of ultrafine grained microstructures on the hot-workability of intermetallic/ceramic composites, Intermetallics, V.9, 2001, 45-49.

154. M. Yamaguchi, S.R. Nishitani, and Y. Srirai, Plastic deformation of intermetallic compoundsTiAl and Al_3Ti, In high temperature aluminides & intermetallics, eds. S.H. Whang, C.T. Liu, D.P. Pope, and J.O. Stiegler, TMS, U.S.A (1990), 63-90.

155. T. Ahmed and H.M. Flower, The phase transformations in alloys based on titanium aluminides Ti_3Al-V and TiAl-V, Mater. Sci. Engg, V.A152, 1992, 31-36.

156. R.G. Rowe, Recent developments in Ti-Al-Nb titanium aluminides alloys, In high temperature aluminides & intermetallics, eds. S.H. Whang, C.T. Liu, D.P. Pope, and J.O. Stiegler, TMS, U.S.A(1990),375-402.

157. Y.W. Kim, and F.H. Froes, Physical metallurgy of titanium aluminides, In high temperature aluminides & intermetallics, eds. S.H. Whang, C.T. Liu, D.P. Pope, and J.O. Stiegler, TMS, U.S.A(1990),465-492.

158. J.M. Larsen, K.A. Williams, S.J. Balsone and M.A. Stuke, Titanium aluminides for aerospace applications, In high temperature aluminides & intermetallics, eds. S.H. Whang, C.T. Liu, D.P. Pope, and J.O. Stiegler, TMS, U.S.A (1990), 521-556.

159. Y. Nishiyama, T. Miyashita, S. Isobe and T. Noda, Development of titanium aluminide turbo-charger rotors, In high temperature aluminides & intermetallics, eds. S.H. Whang, C.T. Liu, D.P. Pope, and J.O. Stiegler, TMS, U.S.A (1990), 557-584.

160. S.J. Zhu, L.M. Peng, T. Moriya, Y. Mutoh, Effect of stress ratio on fatigue growth in TiAl intermetallics at room and elevated temperatures, Mater. Sci. Engg. V.A290, 2000, 198-206.

161. S.H. Wang and Y.D. Hahn, Dislocation structure in $L1_0$ typetitanium aluminides, In high temperature aluminides & intermetallics, eds.S.H. Whang, C.T. Liu, D.P. Pope, and J.O. Stiegler, TMS, U.S.A (1990), 91-110.

162. J. Chraponski, W. Szkliniarz, Quantitative metallography of two-phase titanium alloys, Mater. Char., V.46, 2001, 149-154.

163. F. A. Silva, L.R.O. Hein, J. Ammann and A.M.M. Nazar, Quantitative characterization of multi-phase materials by digiyal Image processing, Prakt. Metallogr.,V.35, 1998, 499-508.

164. P. Belhomme, D. Houivet, W. Lecluse, J. M. Houssonne, Image analysis of multiphased ceramics, J. Eur. Ceram. Soc., V.21, 2001, 2149-2151.

165. B.S.B. Karunaratne, Micromechanisms for plasticity and fracture of Si-Al-O-N ceramics, Ph.D. Thesis, University of Warwick, 1980.

166. H.P.Smith and D.E. Piper, Stress corrosion cracking in high strength steels and in Titanium and Aluminum Alloys, eds. B.F. Brown (Naval Research Laboratory, Washington) V.17, 1992.

A137951